超過冷却液体シリコンの熱物性測定

○岡田純平(宇宙航空研究開発機構 宇宙科学研究所, JST/さきがけ)，石川毅彦，Vijaya Kumar (宇宙航空研究開発機構　宇宙科学研究所)，渡辺勇基（株式会社 エイ・イー・エス）

Thermophysical Properties of Supercooled Liquid Si

Junpei T. OKADA (JAXA/ISAS, JST/PRESTO), Takehiko ISHIKAWA, Vijaya KUMAR (JAXA/ISAS), Yuki WATANABE（AES Co., LTD）

1. Introduction

Silicon (Si) is a key material which plays an important role in semiconductor technology. As crystalline Si is usually generated from the melt, the knowledge of its properties in the liquid and undercooled states is of considerable interest. Physical properties of liquid Si display many unusual aspects. Upon melting, Si transforms into a metal accompanied by a density increased of about 10%. However, the first neighbor atomic coordination number in liquid (l-) Si remains 5.5–6, which is approximately half that of simple liquids metals, hinting that covalent bonds survive even in the metallic state. In fact, molecular dynamics simulations of l-Si at 1800K suggest that approximately 30% of the bonds are covalent [1]. It is remarkable that two completely different types of bonds –metallic and covalent- can coexist in l-Si. The coexistence f two forms of liquid in a single component substance has been predicted to undergo a phase transition as a function of temperature and/or pressure. A recent study reports that l-Si could undergo a liquid-liquid phase transition (LLPT) below 1232K, separating into a high-density metallic liquid and a low-density semimetallic liquid [2]. But, 1232K is far below the melting temperature of 1683K of Si, and as a result the supercooled state has been considered inaccessible to current experimental techniques.

A key requirement for the possibility of an LLPT obviously is that the metallic and covalent bonds coexist in l-Si. Although experimental investigations of the atomic configuration hint at the existence of covalent bonds in l-Si, surprisingly, soft x-ray and magnetic susceptibility measurements of electronic properties so far do not support this viewpoint in that all four valence electrons in l-Si appear to behave like free electrons. Emissivity and thermal conductivity of l-Si also exhibit a free-electron-like temperature dependence. It is clear that the existence of the covalent bonds in l-Si has not been established.

We have performed x-ray Compton scattering experiments on Si using electrostatic levitation technique. An excellent agreement is found between the measurements and the corresponding Car-Parrinello molecular dynamics simulations. The population of covalent bond pairs in l-Si is estimated to be 17% via a maximally localized Wannier function analysis [3]. Our results show persistence of covalent bonding in l-Si and provide support for the occurrence of theoretically predicted LLPT in supercooled states. To realize the predicted metastable phase, we have performed electrostatic levitation experiments on supercooled l-Si.

2. Experiments

Samples were prepared by smashing single crystal wafer Si (99.99999% purity) into small pieces. These pieces were melted into spheroids with 2mm diameter using a gas levitator under Ar atmosphere. The spheroid samples, charged by thermoionic emission, were levitated in a high-vacuum environment (approximately 10^{-5} Pa) using electrostatic forces via a feedback loop. Two horizontal electrodes, separated by 10 mm, assured the vertical position control of the sample. This, together with four spherical electrodes distributed radially at the height of a levitated sample, offered sufficient sample stability to perform measurements of physical properties. The sample was heated and melted using the focused radiation of three laser beams with wavelength of 10.6 μm generated by CO_2 laser. This configuration minimized sample oscillations and enhanced temperature uniformity.

The density l-Si was determined using an ultraviolet imaging technique. The viscosity and surface tension of l-Si were determined by the oscillation drop technique. In this technique, a $P_2 \cos(\theta)$-mode drop oscillation was induced to the liquid sample by superimposing a small sinusoidal electric field on the levitation field. The transient signal that followed the termination of the excitation field was detected and analyzed. This was done several times at a given temperature and repeated for numerous temperatures.

3. Results

Viscosity and surface tension was measured over the temperature range from 1400 to 1700K. Density was measured over the temperature range from 1250 to 1900K. 1250K is very close to 1232K where theoretically predicted LLPT could occur. We will discuss in our talk whether the predicted metastable phase could appear in supercooled Si.

References

1) I. Stich, R. Car, and M. Parrinello, *Phys. Rev. Lett*. 63,2240 (1989)

2) P. Ganesh and M. Widom, *Phys. Rev. Lett*. 102, 075701(2009).

3) J. T. Okada, P. –L. Sit, *et al*.,, *Phys. Rev. Lett*. **108**, 067402 (2012).

「きぼう」搭載静電浮遊炉の開発状況

○田丸晴香，村上敬司，柴崎浩一，大熊隼人，中村裕広，石川毅彦，岡田純平（JAXA），
高田哲也，新井達也，藤野直樹，山浦由起子（株式会社 IHI エアロスペース)

Status of Development of Electrostatic Levitation Furnace (ELF) for KIBO in ISS

Haruka TAMARU, Keiji MURAKAMI, Kohichi SHIBASAKI, Hayato OHKUMA, Yasuhiro NAKAMURA,
Takehiko ISHIKAWA, Junpei T. OKADA (JAXA), Tetsuya TAKADA, Tatsuya ARAI, Naoki FUJINO,
and Yukiko YAMAURA (IHI Aerospace Co. Ltd)

1. Introduction

JAXA has started the development of Electrostatic Levitation Furnace (ELF) for Kibo/ISS. The ELF enable us to realize the containerless processing in a vacuum/gas, and it leads to measurement of thermophysical properties around high melting temperature, and to quest for new functional materials by solidification including overcooling conditions. The first target of ELF for Kibo is the melt oxides. The melt oxides cannot be levitated by electromagnetic force and also it is difficult by ELF on ground, because the electric charge of nonconductor is much less than that of conductor. The ELF will be set into the Multi-purpose Small Payload Rack(MSPR) in Kibo. Fig. 1 shows the overview of ELF.
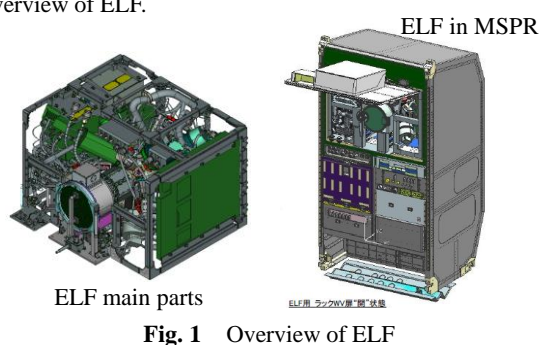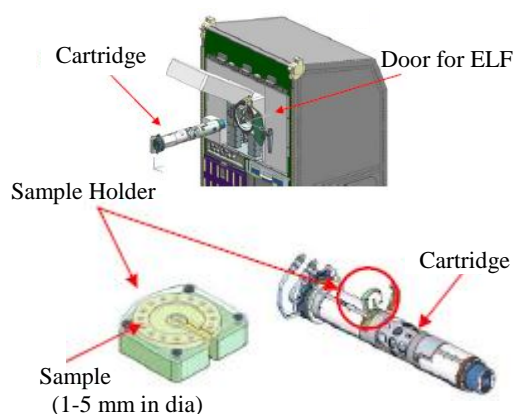

Fig. 1 Overview of ELF

Fig. 2 Sample Cartridge Overview

2. Functions and Specification

2.1 Operation concept

We will launch the sample holder with 15 samples in it. Then the crew will insert/remove that holder into sample cartridge, and install that cartridge into ELF which is shown in fig. 2. If the windows became dirty, the cartridge will be exchanged.

Sample holder (with samples) will be retrieved by any return vehicle.

2.2 Specification

Table 1 shows the engineering Specification of ELF.

Table 1 Engineering Specification of ELF

Items	Spec.
Sample Size	1-5 mm (main target; φ 2mm)
Sample Materials	Metals, Alloys, Glasses, Oxides etc. (Toxic Hazard Level = 0)
Position stability	±100 μm
Atmosphere	Ar / N_2 / N_2+Air up to 2 atm low pressure, 10^{-3} Torr by waste gas line
Heating	970nm / 4 diode lasers. Total 160 W
Temperature measurements	Pyrometer (100Hz), 300~3000℃
Magnified Image	higher than 140 pixel / diameter
Cameras	1 for density measurement (with telephoto lens), 1 for general view
Thermophysical property measurements	・ density by Image Analysis ・ surface tension and viscosity by Oscillating Droplet Method

3. Status of Development

Now we finished the Engineering Model (EM) Fabrication, and we are testing the EM of ELF. It was very difficult to set the EM into the Work Volume of MSPR under various restrictions including the structure, safety, heat exhausting, and power and so on, but finally we completed the fabrication. Fig. 3 shows the assembled EM, and the Levitation control of sample on the ground has realized such as Fig. 4.
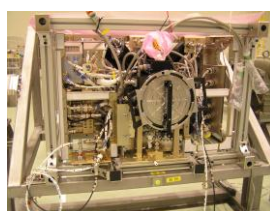

Fig. 3 Assembled EM

Fig. 4 Electrostatic Levitation of EM(φ 2mm glassy carbon)

静電浮遊法による高融点金属の粘性測定

渡邊勇基(エイ・イー・エス)、ヴィジャヤ クマール、岡田純平、石川毅彦
(宇宙航空研究開発機構　宇宙科学研究所)

Viscosity Measurements of Molten Refractory Metals by Electrostatic Levitation Method

Yuki WATANABE (AES), Vijaya Kumar, Junpei OKADA, Takehiko ISHIKAWA (ISAS, JAXA)

1. Introduction

Thermophysical property of refractory metals is important as parameter of numerical simulation for casting, welding, and so on. It is important to know their thermophysical properties for material processing. But there is less or no reliable data due to difficulties of measurement because of their high melting temperature or high vapor pressure.

In recent years, non-contact techniques for thermophysical properties measurements at high temperature with electrostatic levitators (ESL) have been developed [1-3]. Measurements by ESL technique can prevent chemical reactions between the sample and container walls at high temperature.

We understand that viscosity measurement is affected by control frequency to levitate the sample when it overlaps resonance frequency of the sample [4]. In this study, viscosity measurements of molten refractory metals (melting temperature; $T_m > 3000K$) with improved method were attempted.

2. Experimental Setup and Procedures

2.1 Electrostatic Levitation Furnace

The measurements were made using an ESL which consisted of a chamber evacuated to a $\sim 10^{-5}$ Pa vacuum level before processing was initiated. The chamber housed a sample charged by electronic emission and levitated between electrodes via a feedback loop. The two disk electrodes were used for vertical position control whereas four spherical electrodes were dedicated to horizontal control [5]. The positioning control relied on two sets of orthogonally arranged He-Ne lasers and the associated position detectors. Specimens were prepared by arc melting into spheroids with diameters of ca. 2mm.

The sample was heated using two 100W CO_2 lasers split into three beams in a horizontal plane and one 500W YAG laser straight down on the sample. The radiance temperature was measured with a single-color pyrometer.

2.2 Viscosity measurement

The viscosity was determined by the oscillating drop method [6]. In this method, a solid sample was first levitated, rotated around 10Hz, heated, melted, and brought to a selected temperature. Then, a $P_2(\cos\theta)$-mode drop oscillation was induced to the sample by superimposing a small sinusoidal electric field on the levitation field. Using the decay time τ given by the signal, the viscosity η can be determined by:

$$\eta = \rho r_0^2 / 5\tau \qquad (1)$$

3. Results

We measured viscosity of molten refractory metals (Ta, Os, Re, W) which have over 3000K melting temperature. By way of sample, it is shown the viscosity data of molten tungsten (W, $T_m=3695K$) and tantalum (Ta: $T_m=3290K$) measured including undercooled state in wide temperature range in **Fig.1**. It shows viscosity versus temperature with different control frequency of the sample. We were able to measure viscosity of even tungsten (highest T_m in pure metals) in a stable condition due to separating control frequency for levitating and the resonance frequency band of the sample.
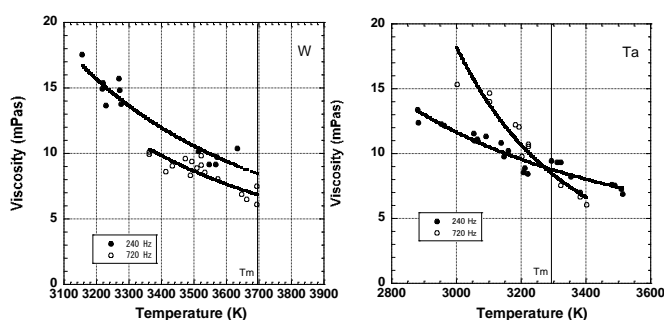

Fig.1　Viscosity of W and Ta versus temperature.

4. Conclusions

The viscosity of molten refractory metals were measured with an electrostatic levitator and the data were reported over wide temperature ranges, including the undercooled state.

References

1) Rhim W K et al. Rev. Sci. Instrum **64** (1993), 2961.
2) P.-F. Paradis and W.-K. Rhim, J. Mater. Res.**14** (1999), 3713.
3) T. Ishikawa, P.-F. Paradis, T. Itami, S. Yoda, Meas. Sci. Technol. **16** (2005) 443-451.
4) T. Ishikawa et al. Rev. Sci. Instrum. **80** (2009), 013906..
5) W. -K. Rhim, S. -K. Chung, D. Barber, K.-F. Man, G. Gutt, A. A. Rulison, and R. E. Spjut; Rev. Sci. Instrum. **64** (1993), 2961.
6) W.-K. Rhim, K. Ohsaka, and P.-F. Paradis; Rev. Sci.Instrum. **70** (1999), 2996.

ガス浮遊法による希土類添加アルミナガラスの生成と光学的特性

○ヴィジャヤ クマール，石川毅彦，岡田純平（宇宙航空研究開発機構 宇宙科学研究所），渡辺勇基（株式会社 エイ・イー・エス）栗林一彦（芝浦工業大学）

Formation and Optical Properties of Rare-earth Aluminates Glass by Aerodynamic Levitation

○Vijaya KUMAR, T. ISHIKAWA, J. T. OKADA (ISAS/JAXA), Y. WATANABE (AES) and K. KURIBAYASHI (SIT)

1. Introduction

Recently, research on bulk glass and glass-ceramics have attracted the attention of material scientists as they are considered as low cost optical materials for the future. Containerless processing enables glass formation of materials with a low glass forming ability because it prevents heterogeneous nucleation from the container walls and thus promotes deep undercooling prior to nucleation from the melt and helps to produce stable, metastable and glass phases. There are few reports on the bulk glass formation of R_2O_3-Al_2O_3 binary system [1-3] but the required properties were not achieved for actual use. The La_2O_3-R_2O_3-Al_2O_3 ternary system was selected in order to fabricate improved properties of new rare-earth aluminate glasses. In the present study, the formation of bulk spherical glasses and their densities, thermal and optical properties have been investigated due to their unique features in terms of the solidification process from an undercooled melt, glass structure and optical properties.

2. Experimental

In order to undercool the melt deeply below the melting temperature, an aerodynamic levitator (ADL) was designed (**Fig.1**). A spherical sample with a diameter of ~2.5 mm and mass of ~20-25 mg was levitated by an ADL and completely melted by a CO_2 laser. The surface temperature and in-situ observation of the levitated droplet was monitored using pyrometer and high speed video camera, respectively. Then the droplet was cooled to room temperature by cutting off the laser.
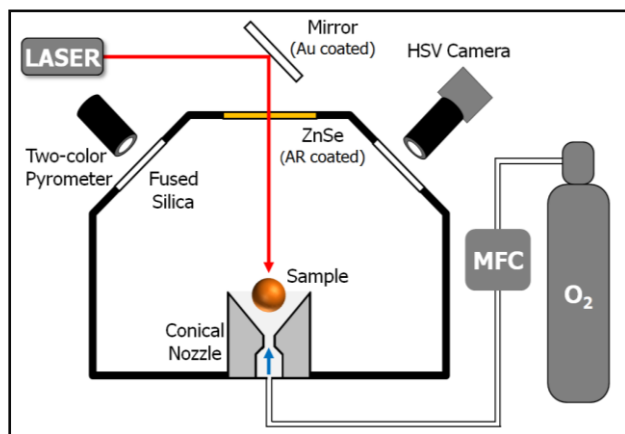

Fig.1 Schematic diagram of an Aerodynamic Levitator (ADL)

The glass transition temperature, thermal stability, density and optical properties were studied for the newly formed glasses.

3. Results and discussion

Figure 2 shows the differential scanning colorimetry (DSC) results of the R_2O_3-Al_2O_3 glasses. The glass transition temperature (Tg) gradually increased with increasing ionic radius of the rare-earth elements. Only one crystallization peak was observed for Nd, where as three crystallization peaks were identified in the Sm-glass. These peaks might be due to the formation of metastable phases. The density decreases with increasing ionic radius and on the other hand the molar volume increases with an increase in the ionic radius. The Nd_2O_3-Al_2O_3 glass showed a high refractive index of ~1.90. These results clearly suggest that the glass with a smaller ionic radius of R has a denser packed structure. Our results indicate that containerless levitation is an elegant technique for fabrication of new glass and crystalline ceramics from an undercooled melt.
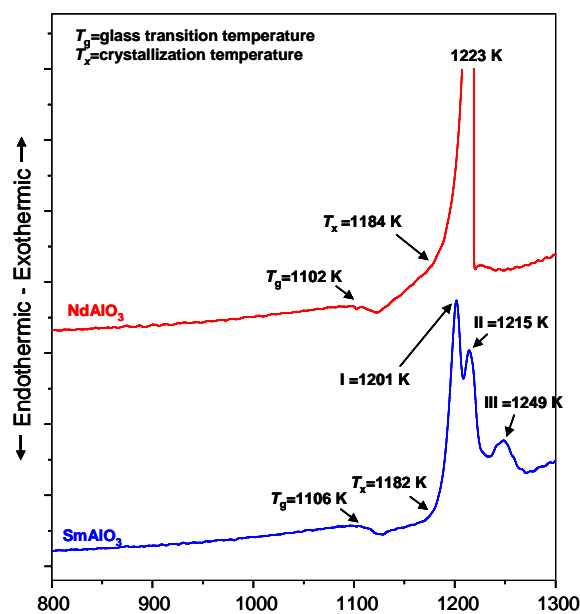

Fig.2 Glass Transition and Crystallization temperatures of the R_2O_3-Al_2O_3 glass determined using DSC.

References

1) J.K.R. Weber, J. J. Felton, B.Cho; Nature, **393** (1998) 769.
2) K. Nagashio et al., Mat. Sci.Forum, **329-330** (2000) 173.
3) C.J. Benmore et al ; J. Phys.Condens. Matter, **41**(2003)S2413.

国際宇宙ステーションでの多元系半導体 InGaSb 結晶成長実験に向けた熱物性測定

○阪田薫穂(JAXA)，向井碧 (AES)，Govindasamy Rajesh，Mukannan Arivanandhan (静大) ，
稲富裕光，石川毅彦(JAXA)，早川泰弘 (静大)

Thermophysical Property Measurements of InGaSb toward the Experiment of Semiconductor Crystal Growth Process on ISS

Kaoruho SAKATA (JAXA), Midori MUKAI (AES Co., Ltd.),
Govindasamy RAJESH, Mukannan ARIVANANDHAN (Shizuoka Univ.),
Yuko INATOMI, Takehiko ISHIKAWA (JAXA), Yasuhiro HAYAKAWA (Shizuoka Univ.)

1. Introduction

The multi-component semiconductor materials are expected to be used for various applications. However, the mechanism of their crystal growth has still many unknown properties for controlling the composition and quality of the crystal, due to segregation related problems and instability of interface between grown crystal and the melt. In order to apply the crystal for device application, it is demanded that the mechanism of crystal growth is clarified. For the purpose, focusing on InGaSb, which can be applied for thermo photovoltaic and infrared detector applications, we are ready to carry out the crystal growth experiment on International Space Station in near future, named "Alloy semiconductor project" [1]. The results of these experiments will be compared with numerical modeling. In order to obtain reliable modeling results, the input parameters i.e., various thermophysical parameters must be accurate. In this study, viscosity of InGaSb was measured, which is an essential property for numerical modeling of crystal growth. In addition, wetting properties between a molten InGaSb and substrates made of quartz, BN, graphite and C-103, used for ampoules and cartridges of the experiments, were investigated. The evaporation rate of molten InGaSb was also investigated to check the affinity of sample configurations.

2. Experimental

The GaSb, InSb and $In_xGa_{1-x}Sb$ samples (x=0.2, 0.4, 0.6, 0.8) were prepared from the 6N purity source materials.

Viscosity was measured with oscillating viscometer (Shinku-Riko, MC980016), and calculated using an approximation method based on the Roscoe's equation [2]. The measurement temperature for $In_xGa_{1-x}Sb$ was set between their melting points and 1100 ℃. BN was used as a crucible material for its high chemical stability and low wetting property for InGaSb.

Wetting property was measured with the 2×2 mm^2 sized $In_xGa_{1-x}Sb$ samples in each composition placed on the substrate material, such as quartz, BN, graphite and C-103 (**Fig.1**). The temperature of the sample was first increased up to just above the melting point in each sample, then the wetting images, wetting angle, and density of the liquid were obtained by changing the temperature to 900 ℃ and 1100 ℃.

For the measurement of evaporation rate, TGA apparatus (Perkin-Elmer TGA7) was used. The sample temperature was kept constant for 180 min at every 100 ℃, between 600 and 1100 ℃. In order to control the sample environment, the experiments were performed under Ar atmosphere.
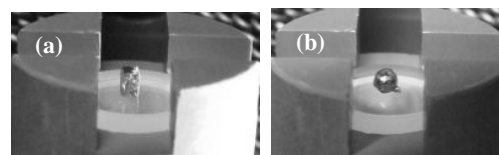
Fig. 1 The sample with the substrate (a) before and (b) after the measurements of wetting property.

3. Results and Discussion

As a result of the measurements, absolute value of viscosity of InSb and GaSb showed good agreement with previous study in literature, and all the results showed good Arrhenius linearity. As for $In_xGa_{1-x}Sb$, it is indicated that the sample with larger component of In showed lower viscosity. These results of viscosity data versus temperature can be applied to the numerical simulations of crystal growth.

From the investigation of wetting property, it is suggested that the wetting ability of InGaSb on C-103 substrate was much higher compared with that on the other substrates (quartz, BN and graphite). The results of BN and graphite having low wetting ability for InGaSb can prove that they are suitable for the ampoule material because they affect little to the crystal growth of InGaSb.

The evaporation rate increased for all the samples by increasing the temperature. At high temperatures, the difference between the evaporation rates of the samples was large.

References

1) M. Arivanandhan, G. Rajesh, A. Tanaka, T. Ozawa, Y. Okano, Y. Inatomi, Y. Hayakawa, Diffusion and Defect Forum, **323-325** (2012) 539.
2) R. Roscoe, Proc. Phys. Soc, **72** (1958) 576.

Acknowledgements

TLZ 法育成 SiGe 結晶大口径化の課題

○木下恭一 [1]，荒井康智 [1]，稲富裕光 [1]，塚田隆夫 [2]，宮田浩旭 [3]，田中涼太 [3]，田口恵祐 [3]，冨岡　浩 [3]，
高柳昌弘 [1]，依田眞一 [1]　　(1: 宇宙航空研究開発機構, 2: 東北大学, 3:（株）エイ・イー・エス)

Issues in Increasing Diameter of TLZ-Grown SiGe Crystals

K. KINOSHITA[1], Y. ARAI[1], Y. INATOMI[1], T. TSUKADA[2], H. MIYATA[3], R. TANAKA[3], K. TAGUCHI[3],
H. TOMIOKA[3], M. TAKAYANAGI[1] and S. YODA[1]　　(1: JAXA, 2: TohokuUniv., 3: AES Co. Ltd)

1. Introduction

We plan homogeneous SiGe crystal growth aboard the ISS using a gradient heating furnace (GHF). The growth method is a traveling liquidus-zone (TLZ) method. The TLZ method is a kind of zone melting method and is proved to be an excellent method for growing compositionally homogeneous mixed crystals such as $Si_{1-x}Ge_x$, $In_{1-x}Ga_xAs$ and so on. For practical use of TLZ-grown crystals, increase in crystal diameter is essential. Here, we report issues in increasing crystal diameter of TLZ-grown SiGe crystals.

2. Experiments

$Si_{0.5}Ge_{0.5}$ crystals were grown by the TLZ method. Crystal diameter were 2, 10, 30 and 50 mm and growth lengths were between 3 and 25 mm. Temperature gradients between 7 and 25℃/cm were applied and growth rates were 0.1 to 0.4 mm/h. Grown crystals were checked by outer shape observation and were characterized by an electron probe microanalyzer (EPMA) and an electron backscattering pattern (EBSP) on polished surfaces.

3. Issues in Increasing Crystal Diameter

Some issues in increasing crystal diameter were found in the course of characterization of various diameter crystals. They are listed below.

3.1 Single Crystal Length Limitation

For 2 mm diameter crystals, 25 mm long $S_{i0.5}Ge_{0.5}$ single crystals were grown[1]. However, single crystal length decreased to about 5 mm for 10 mm diameter crystals[2,3] as shown in **Fig. 1**. This is interpreted that increased convective mixing in a melt caused deeper constitutional supercooling and it resulted in polycrystallization. This hypothesis will be proven by microgravity experiments because convection in a melt is suppressed in microgravity.

3.2 Radial Compositional Variation

In large diameter crystals, radial compositional variation is predicted to be increased by radial temperature gradient[4]. For decreasing radial temperature gradient, thermal conduction control in a sample cell is important. We found that 30 and 50 mm diameter crystals have rather better radial compositional homogeneity than 10 mm diameter crystals. Convective mixing effect in a melt might be beneficial to decreasing radial temperature gradient.

3.3 Cracks

A Si seed is used for growing a $Si_{0.5}Ge_{0.5}$ crystal. Cracks due to lattice mismatch between a seed and a grown crystal, and that between a solidified melt and a feed are inevitable. In addition, cracks due to thermal stress during cooling process after crystal growth increase with increasing crystal diameter. Elimination of cracks may be a critical problem for applying $Si_{0.5}Ge_{0.5}$ crystals to electronic devices.

4. Summary

Some issues in increasing $Si_{0.5}Ge_{0.5}$ crystal diameter is discussed. Microgravity experiments will give a hint to solve some of these issues because convective mixing in a melt is related to some of the issues. The critical problem might be cracks due to lattice mismatch and due to thermal stress. Intensive study is needed for suppressing cracks for applying $Si_{0.5}Ge_{0.5}$ crystals as substrates for electronic devices.
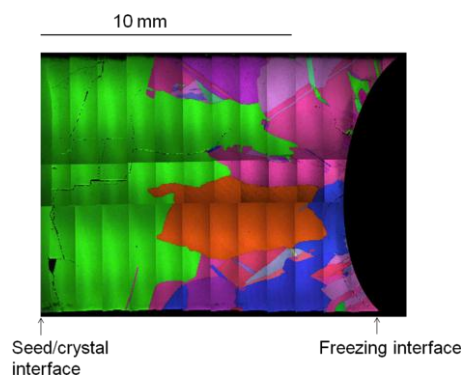
Fig. 1　Crystal orientation analyzed by an EBSP for a 10 mm diameter $S_{i0.5}Ge_{0.5}$ crystal.

References

1) H. Miyata *et al*., J. Crystal Growth, **303** (2007) 607.
2) K. Kinoshita *et al*., Thin Solid Films, **520** (2012) 3279.
3) K. Kinoshita *et al*., J. Crystal Growth, **349** (2012) 50.
4) S. Adachi *et al*., J. Crystal Growth, **334** (2011) 67.

"きぼう"より送られてきているリゾチーム結晶成長"その場"測定データ：
地上と何が違うか

塚本勝男, 忍健太郎, 山崎智也, 三浦均(東北大), 吉崎泉(JAXA), 福山誠二郎(エーイーエス),

島岡太郎(JSF), 真木孝雄(オリンパス(株)), 橘勝(横浜市大), 鈴木良尚(徳島大)

## Live Growth Rate Measurement from Lysozyme Crystals Growing in KIBO

Katsuo Tsukamoto[1], Kentaro Oshi[1], Tomoya Yamazaki[1], Hitoshi Miura[1], Izumi Yoshizaki[2], Seijirou Fukuyama[3],
Taro Shimaoka[4], Takao Maki[5], Masaru Tachibana[6], Yoshinao Suzuki[7]

[1]Grad. School of Science, Tohoku University, Sendai, Japan, [2]JAXA, Tsukuba, Japan, [3]Advanced Engineering Services Co.,Ltd. (AES), [4]Japan Space Forum (JSF), Tokyo, Japan, [5]Olympus Co., Tokyo, Japan, [6]Yokohama City University, [7] Tokushima University

We have successfully been receiving growth rate of lysozyme crystals from "Kibo" at International Space Station (ISS) by *in situ* interferometry since the beginning of August 2012, so as to get the growth rate of lysozyme crystals *vs* supersaturation in an ultra-pure and normal solutions with different protein concentrations. This experiment will continue for the coming five months.

Although so many space grown crystals have been obtained so far, no attempt has been done to measure the growth rate because of two reasons; (1) technical difficulties to measure the growth rate vs supersaturation in space and (2) the growth rate has been believed to be much lower than the rate under gravity due to the absence of convection and flow. However Tsukamoto et al. (2007) found the increase of growth rate of lysozyme crystals by ex-situ measurement in a Foton- M3 recovery satellite in a specific range of supersaturation.

The present experiment is another approach to measure the growth rate *in situ* in the order of 0.01nm/s by interferometry, **Fig.1**, in "Kibo" in order to understand the reason why the growth rate is increased in space. In order to perform this experiment, every parts of "*in situ*" observation systems has extensively been renewed to be miniaturized and simplified with a new concept.
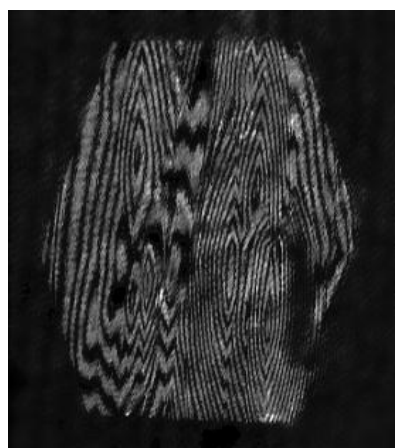
Fig. 1 A live interferogram from a growing lysozyme crystal in KIBO, Michelson Interferogram, to measure the growth rate of crystal with the accuracy of 0.001nm/s.

In the talk, we will review the preliminary results of growth rate vs supersaturation after the review the experimental set-up and finally discuss why the growth rate increased and it is related to the perfection of crystals.

溶液より成長している結晶周囲の三次元濃度場測定

○村山健太，塚本勝男，三浦均，Atul Srivastava (東北大学)，真木孝雄（オリンパス株式会社）

3-D Measurement of the Concentration Field Around Growing Crystal in the Solution

Kenta MURAYAMA, Katsuo TSUKAMOTO , Hitoshi MIURA, Atul SRIVASTAVA (Tohoku Univ.),
Takao MAKI (Olympus Co., Ltd.)

1. Introduction

It is known that the crystal growth mechanism in the solution changes as the supersaturation increases [1]. When the crystal is growing in the supersaturating solution, the solute concentration at the interface is smaller than that of the bulk solution because the crystal grows by incorporating solute in a solution [2].

There have been many reports concerning the measurement of the concentration field, but many of them were two-dimensional (2-D) observations, namely, the objects were observed only from one direction [2]. The information obtained by the 2-D observations is integrated along the direction of the observation, so the local information, e.g., concentration distribution around the crystal-liquid interface, was not obtained.

2. 3-D observations

To improve the disadvantage on the 2-D observation, a method of computer tomography (CT) has been adopted by some authors. By using the CT method, one can reconstruct the information of the three-dimensional (3-D) concentration field around the growing crystal based on 2-D observations obtained from several directions (3-D observation) [3].

Srivastava *et al.* (2010) carried out a 3-D observation of the concentration field around sodium chlorate using Mach–Zehnder interferometer and octagonal crystal growth cell. The octagonal cell enables us to obtain interferograms in four different directions (0, 45, 90, 135 degree) [4].

However, the spatial resolution in tomography will be improved by increasing the number of the observation directions. It is necessary to discuss whether the observation from four angles is enough for measuring the concentration field or not, so the observation from more directions is desirable.

3. Refractive index matching cell

To obtain 2-D images in many directions, we prepared a cylindrical growth cell. Usually, it is considered that the cylindrical cell is not suitable for the interferometer because the curved wall of the cell bends the light beam. We will overcome this problem by using the refractive index matching method [5].

To avoid the bending of the light beam, we put the matching liquid whose refractive index is close to that of the glass around the cylindrical cell. This liquid removes refraction and reflection of the light at the wall of the cylindrical cell, so the beam can pass through the cell straightly (**Fig.1**).
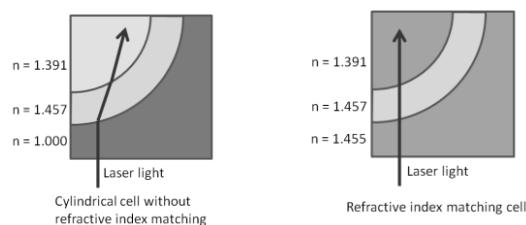

Fig.1 Principle of refractive index matching

4. Results and discussions

We observed the concentration field around sodium chlorate (NaClO$_3$) crystal growing in the solution. The supersaturation was adjusted at σ =0.0335 in bulk. The observation was carried out at intervals of 22.5 degrees. **Fig.2** shows the comparison of the interferograms in the case of only the cylindrical cell (a) and the refractive index matching cell (b). In **Fig.2** (a), the obtained interference fringes were not suitable for determining the concentration distribution because of the refraction of the light and the influence of aberration by the lens effect at the cell wall. In **Fig.2** (b), we obtained the interference fringes at equal interval at the bulk solution, which enable us to determine the concentration field. These results suggested that the matching liquid removed the bending of the light beam properly. By using the cylindrical growth cell with the refractive index matching method, the observation from arbitrary angles became possible.

The number of the observation directions can be increased by using the refractive matching cell. It is expected to improve the spatial resolution of 3-D observation of a concentration field.
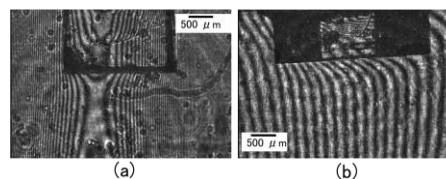
Fig. 2 Interferograms of the concentration field around NaClO$_3$ crystal (a) Cylindrical cell in the raw(b) Refractive index matching cell

References

1) Ichiro Sunagawa. Kyoritsu publishing, 2003.
2) Shigenao Maruyama, Toshiyuki Shibata, Katsuo Tsukamoto and Kenji Shimizu: Heat Transfer-Japanese Research, **27 (2)** (1998) 114
3) F. Bedarida: J. Crystal Growth, **79** (1986) 43
4) Atul Srivastava, Katsuo Tsukamoto, E. Yokoyama, K. Murayama, M. Fukuyama: J. Crystal Growth, **312** (2010) 2254
5) Hiroyuki Suhara, Satoru Itoh, Takeshi Ueda and Tatsuya Ito: Ricoh Technical Report, **25** (1999) 120

タンパク質結晶化容器 JAXA Crystallization Box (JCB)の改良

○田仲広明，厳　斌（（株）コンフォーカルサイエンス CS），古林直樹（（株）丸和栄養食品 MF），
高橋幸子（CS），正木美佳（（独）宇宙航空研究開発機構 JAXA），伊中浩治（MF），太田和敬，
小林智之，三好寛、吉村善範（JAXA）

Upgrade Version of JAXA Crystallization Box (JCB) for Protein Crystal Growth in Space

Hiroaki TANAKA, Bin YAN (CS), Naoki FURUBAYASHI (MF), Sachiko TAKAHASHI (CS), Mika MASAKI (JAXA),
Koji INAKA (MF), Kazunori OHTA, Tomoyuki KOBAYASHI, Hiroshi MIYOSHI, Yoshinori YOSHIMURA (JAXA)

1. Introduction

JAXA Crystallization Box High Density (JCB-HD) has been the main crystallization device in JAXA High-quality Crystallization Project since 2007. JCB-HD is a cell with high density integration, using the counter-diffusion method. However, it has some points to be improved such as non-negligible water permeability, smaller volume of precipitant solution cells, and rather complicated assembly. To solve these points, we are now developing a new cell, JAXA Crystallization Box (JCB)-SGT.

2. New Crystallization Device

2.1 JCB-SGT

The outlook of JCB-SGT is shown in **Fig. 1**. JCB-SGT is made of very low water-permeable material, Techbarrier-HX (PET+SiOx coating). Therefore water permeability of the crystallization cell which may cause air bubbles in the precipitant cell will not disturb crystallization in JCB-SGT. JCB-SGT can contain much larger volume of precipitant solution in one cell (1200 micro-L) if compared to JCB-HD (180 micro-L). Therefore, the amount of the precipitant solution in JCB-SGT is large enough not to worry about the dilution of the precipitant solution with protein solution during the crystallization experiment.


Fig. 1 Outlook of JCB-SGT

The preparation of JCB-SGT is shown in the **Fig. 2**. There are three thin and long cells in one SGT Crystallization Unit. The cell is filled with precipitant solution. The capillary filled with protein solution is plugged with "gel-tube" and inserted in the cell. The capillary is 40 mm in length and 0.5 mm in diameter. The end of the capillary is sealed with clay and the other end with an agarose gel in the "gel-tube". Two capillaries can be inserted in one cell. Then three cells are sealed together with sealing machine. JCB-SGT is composed of two SGT Crystallization Units (12 capillaries), which means the volumetric efficiency is the same as JCB-HD. The lysozyme crystal grown in JCB-SGT is shown in **Fig. 3a**.

2.2 JCB-SLC

JCB-SLC is a device for growing larger crystal. The
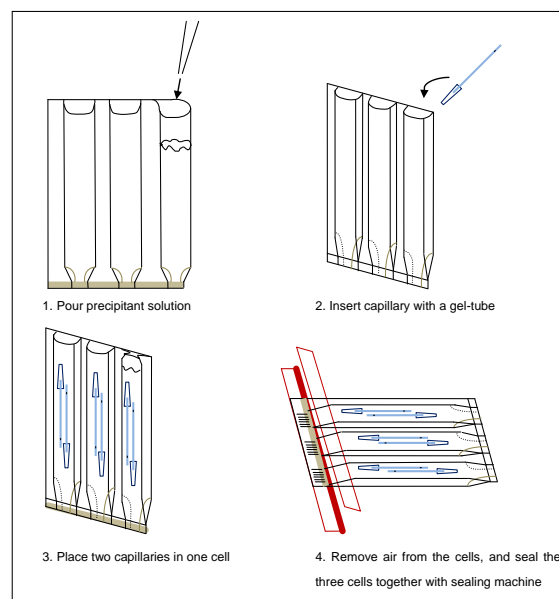
Fig. 2 The assembly of JCB-SGT
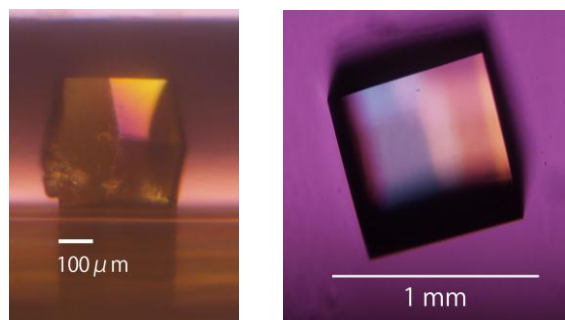
Fig. 3 Crystals grown in (a) JCB-SGT and (b) JCB-SLC

crystallization cell is the same as JCB-SGT. Instead of the capillary of 40 mm in length, shorter capillary of 35 mm in length with larger bore of 1.9 mm is used. The preparation of JCB-SLC is as the same as JCB-SGT except one capillary in one cell. After insertion, three cells are sealed together with sealing machine. JCB-SLC is composed of two SLC Crystallization Units (6 capillaries). The assembly of JCB-SLC is easier than that of JCB-MC (former type of crystallization cell for larger crystal). The large lysozyme crystal grown in JCB-SLC is shown in Fig. 3b.

These new crystallization devices will be in use in JAXA PCG#6, 2013 (TBD).

ダストプラズマにおける粒子温度計測

○足立 聡 (宇宙航空研究開発機構 (JAXA))，東辻浩夫 (JAXA，岡山大学)，
高橋和生 (京都工芸繊維大学)

Particle Temperature Measurement in Complex Plasmas

Satoshi ADACHI (Japan Aerospace Exploration Agency (JAXA)), Hiroo TOTSUJI (JAXA and Okayama Univ.),
Kazuo TAKAHASHI (Kyoto Institute of Technology)

1. Introduction

Particle temperature, being equivalent to average kinetic energy, in complex plasmas is usually estimated from the velocity distribution function (VDF). To obtain the VDF is not easy in many cases since the statistical reliability is required. To satisfy the reliability, the large number of particles must be observed. This corresponds to the large observation area by using a small magnification lens. However, the larger area makes the worse velocity resolution. This means that it is more difficult to recognize the correct profile of the VDF. Hence, we investigated a new method of measuring the particle temperature based on the pair distribution function (PDF).

2. Theory and Results

The PDF for the complex plasmas is described as

$$g(r) = \sum_h \sum_k \sum_\ell \exp\left\{-2\pi^2 \left\langle (\Delta x)^2 \right\rangle \times \left(h^2 + k^2 + \ell^2\right)\right\} \times \exp\left\{2\pi i \left(hx + ky + \ell z\right)\right\} \quad , \tag{1}$$

where h, k and ℓ are the Miller indices, x, y and z are the coordinates in the unit cell, $\left\langle (\Delta x)^2 \right\rangle$ is the mean square displacement (MSD). The exponential function having the MSD is called the temperature factor or Debye-Waller factor, representing the temperature influence on the PDF. This means that the temperature is basically estimated from the PDF. If the displacement Δx is expressed by a normal distribution and

particle oscillations are approximated to be harmonic oscillations, the temperature in two-dimensional cases like the complex plasmas on the ground should be described [1] as

$$k_B T = m \left\langle (\Delta x)^2 \right\rangle \sum_n \omega_n{}^2, \tag{2}$$

where ω_n represents the oscillation frequency.

The oscillation frequencies are obtained by tracing particle motions and calculating the Fourier spectra of the time evolutions of the particle coordinates. The typical result is shown in **Fig. 1**. From the figure, it is found that the fundamental frequencies are 0.64 and 0.88 Hz and the second harmonics are 1.29 and 1.64 Hz. Thus the temperature is estimated to be 0.29 eV, which is reasonable value as compared with the temperature from the velocity distribution function method.

The two fundamental frequencies may suggest anisotropy though the complex plasmas are considered to be an almost ideal isotropic system. Therefore, further investigation is needed to understand the particle oscillations. One possibility causing the anisotropic oscillation may be the defects. To investigate the defects, we trace the dislocation as the first step. **Figure 2** shows the typical result of the dislocation detection. It is clearly observed that the dislocations move around and lattice distortions relax over time.

References

1) S. Adachi, H. Totsuji, K. Takahashi, Y. Hayashi and M. Takayanagi: J. Phys.: Conf. Ser., **327** (2011) 012043.
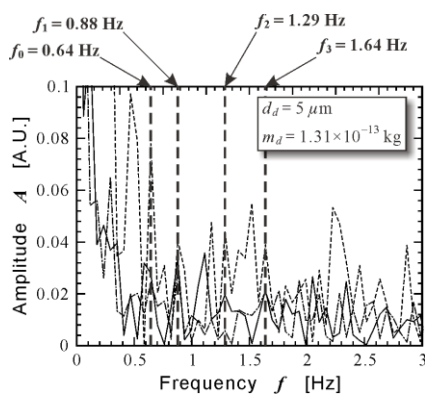
Fig. 1 Typical result of oscillation frequencies
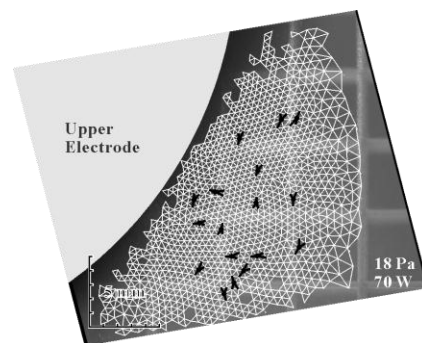
Fig. 2 Typical result of dislocation detection

ISS/JEM 内の微小重力環境

○石川巨樹 (株式会社エイ・イー・エス)，柴崎浩一，大熊隼人 (宇宙航空研究開発機構)

Microgravity Environment in ISS/JEM

Naoki ISHIKAWA[1], Kohichi SHIBASAKI[2], Hayato OHKUMA[2]
1. Advanced Engineering Services, Co., Ltd.   2. Japan Aerospace Exploration Agency

1. Introduction

In the International Space Station (ISS) / Japanese Experiment Module (JEM), various kinds of experiments have been performed using a microgravity environment. However, this microgravity environment is disturbed due to the vibration which occurred by crew activity, experimental equipments and docking of vehicles, etc [1,2]. Thus we have been measured microgravity environment in JEM by Microgravity Measurement Apparatus (MMA) and investigated amplitude and sources of vibration for user by analyzing measured data.

In this investigation, we show the characteristic of disturbance. And we approach analysis of the time dependence of disturbance in JEM in order to inform user of microgravity environment in JEM.

2. Microgravity Measurement Apparatus (MMA)

The MMA is consists of following four devices:

TAA (Tri-axial Accelerometer Assembly)
RSU (Remote Sensor Unit)
NCU (Network Control Unit)
MLT (MMA Laptop Terminal)

TAA is located on the surface of SAIBO, RYUTAI and KOBAIRO racks in JEM. Overview of the MMA configuration in JEM is shown in **Fig. 1**. Mainly, we use the MMA of RYUTAI Rack for measurement of microgravity. Data shown in section 3 is also measured here.
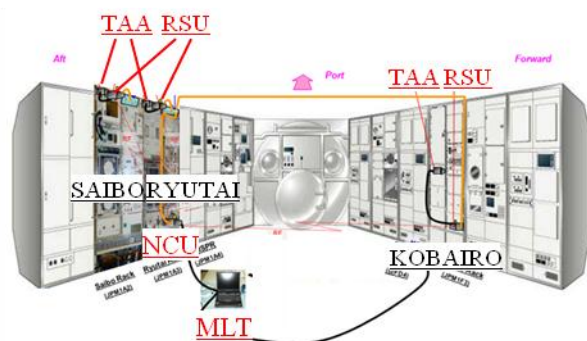

Fig. 1 Overview of the MMA

3. MMA Data Analysis

We show the analyzed data taken by one day in **Fig. 2**. It shows relations between time and acceleration of three frequencies (1, 20 and 100 Hz). Here, points of data in **Fig. 2** are calculated by 1/3 octave band analysis per an hour, so absolute value of acceleration is unconsidered.

According to **Fig. 2**, it is discern that fluctuation of 1 Hz acceleration is larger than the others. Because disturbance at 1 Hz is caused by crew activity, so acceleration is decreased during crew sleep. On the other hand, high frequencies (20 and 100 Hz) are not decreased through 1 day. This is because the source of vibration is in the apparatus which is always working.
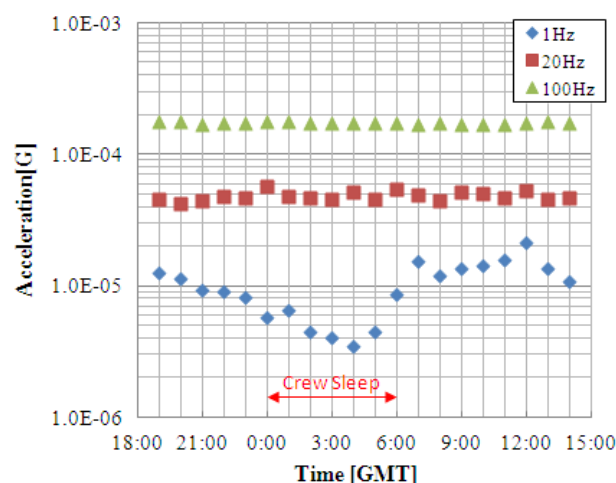

Fig. 2 Relations between time and acceleration

4. Conclusion

We showed relation between time and acceleration in one day.

Hence we will analyze in detail more data to indicate the general microgravity environment in JEM from a statistical point of view. Moreover, we will examine the variation of disturbance in the long term.

References

1)   M. Goto, K. Murakami, H. Ohkuma: J. Micro. Soc. **Vol.28 No.1** (2011) 8.

2)   H. Ohkuma, K. Murakami, M. Goto: J. Micro. Soc. **Vol.28 No.1** (2011) 13.

大気球を利用した液滴列の微小重力燃焼実験

石川毅彦，○菊池政雄（JAXA），山本信（㈱IHI エスキューブ），澤井秀次郎，丸祐介，橋本樹明，
坂井真一郎，坂東信尚，清水成人，小林弘明，吉光徹雄，菅勇志，田崎彩（JAXA），
福山誠二郎（㈱AES），岡田純平，依田眞一，福家英之，梯友哉（JAXA）

Droplet Array Combustion Experiment in Microgravity by Using Balloon Operated Vehicle

Takehiko ISHIKAWA, Masao KIKUCHI (JAXA), Shin YAMAMOTO (IHI Scube Co., Ltd.), Shujiro SAWAI,
Yusuke MARU, Tatsuaki HASHIMOTO, Shinichiro SAKAI, Nobutaka BANDO, Shigehito SHIMIZU, Hiroaki
KOBAYASHI, Tetsuo YOSHIMITSU, Yuuji KAN, Aya TAZAKI (JAXA), Seijiro FUKUYAMA (AES Co., Ltd.),
Junpei OKADA, Shinichi YODA, Hideyuki FUKE, Yuya KAKEHASHI (JAXA)

1. Introduction

Droplet array combustion experiment in microgravity environment, provided by the balloon operated vehicle, has been prepared by the authors. In this paper, overview of the experiment and the latest status are reported.

2. Overview of the Experiment

2.1 Objectives

Primary objective of the experiment is demonstration and verification of the modified experimental system by the balloon operated vehicle, described in 2.2, for microgravity experiments in the future. Secondary objective of the experiment is acquisition of experimental data on fuel droplet array combustion in microgravity. Kikuchi et al., have performed study on flame spread mechanism along linear fuel droplet array in microgravity by using drop shaft, parabolic flight, and sounding rocket. In recent sounding rocket experiment by TEXUS rocket, the effects of partial pre-vaporization of droplets on flame spread and combustion characteristics were examined [1]. However, there is lack of experimental data with medium degree of pre-vaporization, though data with small and large degree of pre-vaporization were successfully obtained by the drop shaft experiments and by the sounding rocket experiment, respectively. Therefore, acquisition of experimental data with medium degree of pre-vaporization is intended by the current experiment by the balloon operated vehicle.

2.2 Experimental System

The experimental system is based on that used in previous missions [2]. However, it was vigorously modified this time so that it could accommodate much larger payload in the main body, compared with previous missions. Also, drag-free control method for the payload was changed from previous 3-axis method to 1-axis method, as shown in **Fig. 1**. Engineering model (EM) of the droplet array combustion experiment unit (DCU) for the previously mentioned TEXUS rocket experiment is employed as the payload in the current experiment. Some modifications of the DCU EM (e.g. Replacement of high-speed video camera, Addition of electric batteries, etc.) was performed

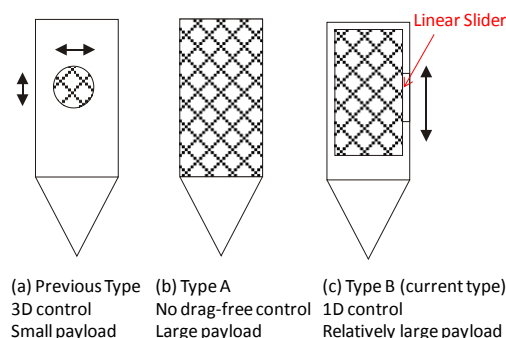for the experiment. Appearance of the modified DCU EM is shown in **Fig. 2**.

(a) Previous Type
3D control
Small payload

(b) Type A
No drag-free control
Large payload

(c) Type B (current type)
1D control
Relatively large payload

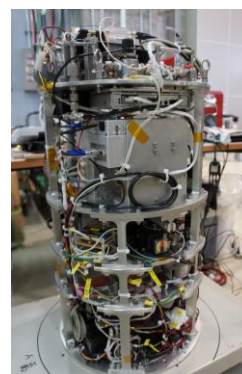**Fig. 1** Drag-free control method of the payload

Fig. 2 Appearance of the DCU EM

3. Latest Status of the Experiment

Development of the whole experimental system was completed by the summer of 2012. Final preparation of the experiment was also performed in the experimental site (Taiki town, Hokkaido) from mid. August, 2012. Unfortunately, however, execution of the flight experiment in this season was cancelled, due to undesirable wind condition in the high altitude.

References

1) M. Kikuchi, et al., *Proc. 49th Combustion Symposium (Japanese)*, pp.108-109, 2011.
2) S. Sawai, et al., *J. Jpn. Soc. Microgravity Appl.*, **26** (2009)21-28.

微小重力場における電線被覆の過電流連続通電による着火限界

○重田尚樹，伊東弘行，藤田修（北海道大学大学院）

Ignition Limit of Electric Wire Insulation with Continuous Excess Current in Microgravity

Naoki SHIGETA, Hiroyuki ITO, Osamu FUJITA (Hokkaido Univ.)

1. Introduction

Overloading of an electric wire is a cause of fire in space craft. Wire ignition by overloading is more probable in microgravity (μg) than normal gravity (1g) according to previous works [1,2]. Therefore, it is important to know the ignition characteristics of overloaded wires in μg.

The ignition limit is defined as the lowest applied power at which ignition can occur. According to the previous research, the ignition limit decreases when microgravity time is increased [2]. So it is important to know the real ignition limit in long term μg environment. In the present work, therefore, the effect of μg time on this limit is investigated by parabolic flight experiments.

2. Experimental

The experimental system is shown in **Fig.1**. This system consists of the combustion chamber, the sample holder with sample wire, the power source, the programmable controller, and a digital video camera (30 fps). The combustion chamber is air tight structure, in which wire ignition takes place. A series of several experiments are held without gas displacement, so absorber of combustion products, CO_2 and H_2O, is set in the chamber. Initial O_2 concentration is 21%, and balance gas N_2, total pressure 100kPa. Sample wire is a nickel-chrome core wire coated with polyethylene insulation, because it is easy to control the value of the Joule energy given for the wire. The diameters of the wire and inner core are 0.8 and 0.5 mm, respectively. The electric current is a main test parameter, which is kept constant for the period of a parabolic flight test. Microgravity experiments were held at Diamond Air Service (DAS) in Komaki, Aichi. The available microgravity time by a parabolic flight is around 20s.
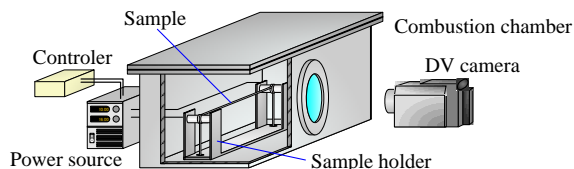

Fig.1 Experimental setup.

3. Results and discussion

Fig.2 shows relationship between ignition delay time, defined as the time after the start of the current supply until the moment of ignition, and applied power per unit length, which is computed by multiplying square current by resistance. The data

obtained by a drop tower and in 1g are from the previous work [2]. Ignition delay time increases when applied power was decreased. The ignition limit also decreases as μg time increases. **Fig.3** shows a comparison of minimum ignition energy, defined as total energy for ignition, between 1g and μg. This energy in μg is lower than in 1g. And in μg, despite ignition delay time being greatly changed the energy changes not significantly. It implies that the wire ignites if a given Joule energy is supplied to the wire in μg, which is smaller than that in 1g.
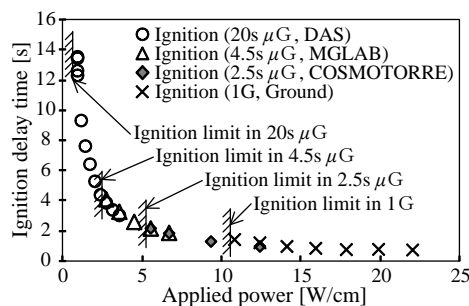

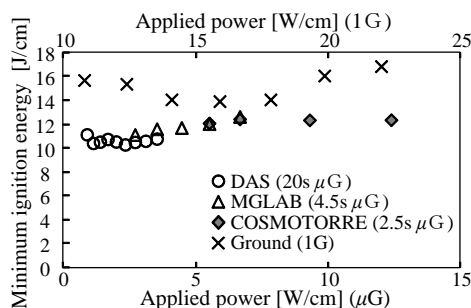**Fig.2** Ignition delay time (DAS:O_2=19-21%, Others: O_2=21%)

Fig.3 The difference in minimum ignition energy between 1g and μg (DAS:O_2=19-21%, Others: O_2=21%)

4. Conclusions

In μg, the ignition limit decreases when μg time increases. However, in any μg time, minimum ignition energy is not significantly changed. It means that a minimum amount of Joule energy is required for ignition, which can be called as minimum ignition energy for wire insulation.

References

1) R. Friedman, Fire Safety in Spacecraft, FIRE AND MATERIALS, **20**(1996) , 235

2) K.Agata, Y.Ichimura, T.Fujii, H.Ito, Y.Naokamura, O.Fujita ., 45th Japanese combustion symposium(2007), 468

赤外吸収法を用いた燃料液滴近傍の蒸気濃度計測

○福山誠二郎((株)エイ・イーエス)，菊池政雄(JAXA)，山本信 ((株)IHI エスキューブ)

Study on Fuel Vapor Concentration Measurement near Fuel Droplet Surface by Infrared Laser Absorption Method

Seijiro Fukuyama (AES Co., Ltd.), Masao Kikuchi (JAXA), Shin Yamamoto (IHI Scube Co., Ltd.)

1. Introduction

It is essential to consider the influence of pre-vaporized fuel vapor layer around fuel droplets on flame spread between droplets, from the viewpoint of flame spread in spray combustion for low volatility fuel in high-temperature atomsphere, such as internal combustion engine. Investigations on fuel droplet-array combustion have been conducted by microgravity experiments for research on essential mechanism of spray combustion [1]. In this study, measurement of fuel vapor concentration near the surface of fuel droplet was performed by using the infrared laser absorption method [2].

2. Experimental

2.1 Principle of method

The Basic principle of the infrared laser absorption method is expressed as

$$\log\left(\frac{I}{I_0}\right) = -\varepsilon\, c\, L \qquad (1)$$

where I_0 and I are intensity of incident light and transmitted light, ε is molar absorption coefficient, c is mol concentration, and L is optical path length, respectively. The equation (1) is called the Lambert-Beer Law. Hydrocarbon molecules such as n-decane have characteristic absorption wavelength at 3.39 μm, which is based on stretching vibration of the C-H band.

2.2 Experimental set-up

Schematic of the experimental set-up is shown in **Fig.1**. He-Ne laser with 3.392 μm (NEOARK, NEO-30R3) is employed as infrared light source in this study. Laser beam is condensed by a condenser lens into the diameter of tens of micrometers at a focal point. The light which passes near n-decane droplet surface is led to a bandpass filter and detected by an IR detector. Detected data is collected with a data recorder.
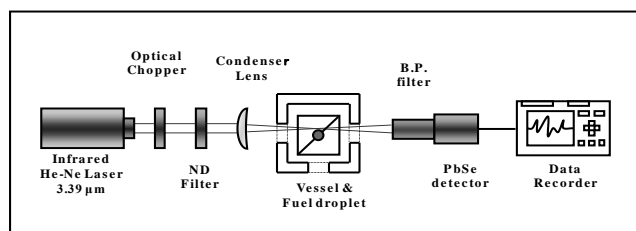

Fig. 1 Schematic of experimental set-up.

3. Experimental

3.1 Preliminary Experiment

Prior to the measurement of fuel vapor concentration around fuel droplet, ε shall be decided. For that, saturated vapor condition at different ambient temperatures was employed. Since c (equivalence ratio) and L are known at the saturated temperature, ε can be decided through measurement of the (I / I_0) and the averaged value of $\varepsilon = 8.7 \times 10^{-3}$ ($1 / \phi \cdot$mm) was employed for the measurement of n-decane fuel vapor concentration.

3.2 Principal Experiment

The measurement results, on the amount of laser absorption near droplet surface for different ambient temperatures with n-decane, indicate that the intensity of the transmitted laser decreases with approach to the droplet surface for increase of fuel vapor concentration. Also, it is seen that the amount of laser absorption at a specific distance from the droplet surface increases with ambient temperature. It could be attributed to the development of fuel vapor layer around the droplet with increase of ambient temperature. It was shown that infrared laser absorption method could be applied to measurement of distribution of fuel vapor concentration around fuel droplets by scanning the laser path.

4. Summary

These experiments revealed that infrared laser absorption method could be applied to measurement of distribution of fuel vapor concentration around fuel droplets.

Furthermore, from the viewpoint of comparison 1g and μg, the similar principle of infrared laser absorption measurements were performed for 2.5 s microgravity experimental facility (COSMOTORRE) located in Hokkaido, Japan. Unfortunately, for large noise were observed, it could not be obtained the reliable results.

References

1) Kikuchi et al., 6th Asia-Pacific Conference on Combustion 639-642 (2007).

2) Edwards, B. et al., J. Opt. Soc. Am., Vol.55, No.2, 174-177 (1965).

ISS「きぼう」における固体材料燃焼実験（Solid Combustion）

○田﨑彩，菊池政雄，高柳昌弘（JAXA），藤田修（北海道大学），高橋周平（岐阜大学），
伊藤昭彦，鳥飼宏之（弘前大学）

Overview of "Solid Combustion" experiment in the ISS/KIBO

Aya TAZAKI, Masao KIKUCHI, Masahiro TAKAYANAGI (JAXA),Osamu FUJITA (Hokkaido Univ.),
Shuhei TAKAHASHI (Gifu Univ.), Akihiko ITO, Hiroyuki TORIKAI (Hirosaki Univ.)

1. Itroduction

A lot of astronauts have been staying in spaceship or the International Space Station(ISS) for long term and we have been carring out many scientific experiments in the microgravity environment. Therefore, it is important issue to protect astronauts from fire in the microgravity environment. However the current material flammability tests for fire safety in space are attained in normal gravity, and it is known that the material flammability could be higher in microgravity in some conditions[1]-[4]. Thus it is necessasry to understand the impact of gravity presence on material flammability.

2. Overview of the Experiment

2.1 Objectives

"Quantitative Description of Gravity Impact on Solid Material Flammability as a base of Fire Safety in Space(Solid Combustion)" is one of the candidate experiments of Japanese Experiment Module/KIBO in the ISS. The Solid Combustion experiment is planned to conduct using the Multi-purpose Small Payload Rack(MSPR). In the present research, three types of solid material, polyethylene insulated wires, flat plastic sheets and filter papers are selected as test samples and their flammability regarding two fundamental processes of solid combustion, that is, (1)solid material ignition, and (2)flame spread over solid material, will be quantitatively determined in microgravity. Then, the discussion on the discrepancy between the data in normal and micro gravity will be made to give the validity of the current material flammability tests.
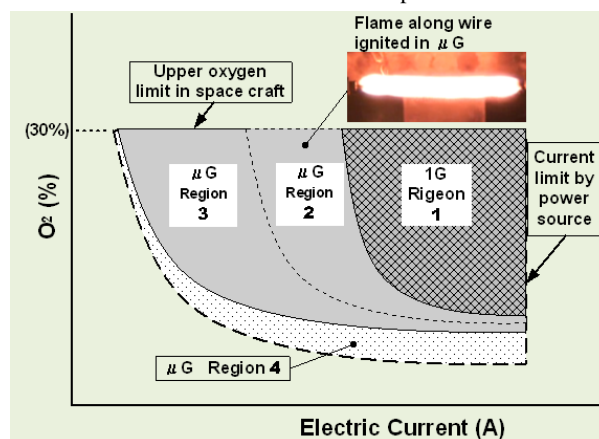
2.2 Map of ignition and flammability

Fig.1 shows a conceptual description of ignition map of overloaded polyethylene insulated wire in terms of O2 concentration and electric current. It is already known that the ignition limit is extended in microgravity. **Fig.2** conceptually describes the condition where spreading flame is sustained. The extinction limit(LOI) will be extended in microgravity. But it is difficult to complete ignition map and flammability map and to determine the actual limit without long-term microgravity experiments.

2.3 Status of the Experiment

We are developing a combustion device which enables experiments for the above mentioned three material types. It is possible to change oxygen concentration, electric current and air flow velocity by the device. Here, we provide an overview of recent status of the Solid Combustion experiment.
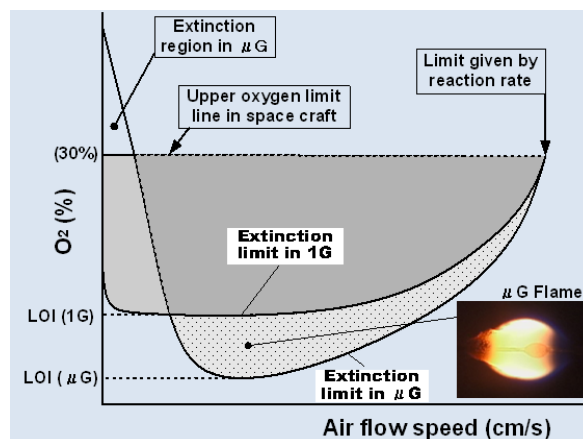

Fig.1 Ignition map of overloaded wire

Region1:Ignition limit in 1g.
Region2:Ignition limit in short-term μg tests.
Region3:Ignition limit in long-term μg tests.
Region4:Ignition but no sustained flame.

Fig.2 Flammability map of spreading flame

LOI : Low oxygen index minimum O2 concentration to sustain flame spreading.

References

1) K. Agata, et al., *J. Jpn. Soc. Microgravity Appl.*, **Vol.25 No.1**, pp. 11-16, 2008.1.

2) O. Fujita, *J. Jpn. Soc. Microgravity Appl.*, **Vol.28 , No.3**, pp. 90-95, 2011.

3) Y. Onishi, et al., *Transactions of the Japan Society for Aeronautical and Space Sciences*, **Vol.8**, pp.Ph_19-Ph_24, 2010.

4) O. Fujita, et al., *Proc.Combustion Institute,* **Vol.33, Issue2**, pp.2617-2623, 2011.

微小重力下での超臨界二酸化炭素中における不斉光反応

西山靖浩 (奈良先端科学技術大学院大学)，夏井坂誠 (宇宙航空研究開発機構)，辻井薫 (北海道大学)，
垣内喜代三(奈良先端科学技術大学院大学)，出口茂 (海洋研究開発機構)，○井上佳久(大阪大学)

Effects of Microgravity on Chiral Photoreaction in Supercritical Carbon Dioxide

Yasuhiro NISHIYAMA (Nara Institute of Science and Technology), Makoto NATSUISAKA (Japan Aerospace Exploration Agency), Kaoru TSUJII (Hokkaido Univ.), Kiyomi KAKIUCHI (Nara Institute of Science and Technology), Shigeru DEGUCHI (Japan Agency for Marine-Earth Science and Technology), Yoshihisa INOUE (Osaka University)

1. Introduction

Chiral photochemistry, which allows us to produce optically active compounds through electronically excited state, becomes more popular in recent years as an alternative to the thermal asymmetric syntheses that employ conventional ground-state chemistry. Of several chiral photochemical strategies, the enantiodifferentiating photosensitization, using only a catalytic amount of chiral sensitizer, is particularly attractive from the viewpoint of chiral-source efficiency.

We investigated the enantiodifferentiating photoisomerization of (Z)-cyclooctene (**1Z**) sensitized by pyromellitates (**Pyro**) with optically active menthyl (**Men**), 8-phenylmenthyl (**8Ph-Men**) and diacetone fructose (**DAF**) auxiliaries (**Fig. 1**) in organic solvents to reveal that the enantiomeric excess (ee) of chiral photoproduct, (E)-cyclooctene (**1E**), is a linear function of pressure (at least from 0.1 to 400 MPa).[1]
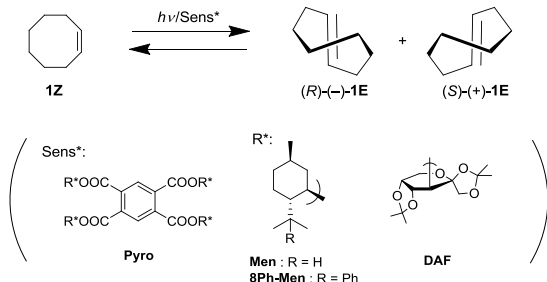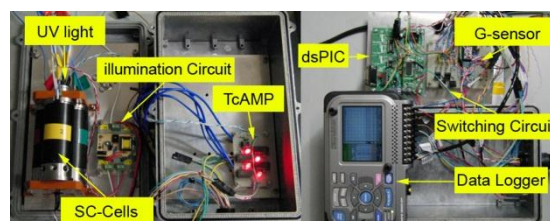

Fig. 1 Enantiodifferentiating photoisomerization of (Z)-cyclo-octene (**1Z**) sensitized by pyromellitates (**Pyro**).

Interestingly, the ee of **1E** obtained was not linear to pressure but showed a sudden leap near the critical density when the photosensitization was run in near- and supercritical carbon dioxide (nc/scCO$_2$).[2] The unique photobehavior in nc/scCO$_2$ was related to the change in CO$_2$ clustering around the excited-state complex of substrate with sensitizer and therefore affected by the density fluctuation of nc/scCO$_2$ media. This observation prompted us to examine the effect of microgravity (μg) on the chiral photoreaction in nc/scCO$_2$, where the clustering behavior is expected to be varied under μg.
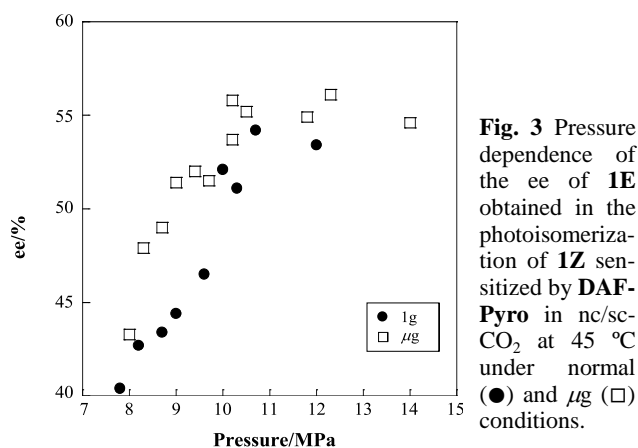
2. Results and Discussion

First, we developed a transparent cylindrical pressure vessel made of sapphire tube (1 mL net volume), which was designed for performing photoreaction under μg in a parabolic flight (**Fig. 2**); see the related abstract by Natsuisaka et al. for detail.

Fig. 2 The system developed for the photoreaction under μg.

Fig. 3 Pressure dependence of the ee of **1E** obtained in the photoisomerization of **1Z** sensitized by **DAF-Pyro** in nc/sc-CO$_2$ at 45 ℃ under normal (●) and μg (□) conditions.

The enantiodifferentiating photoisomerization of **1Z** sensitized by **DAF-Pyro** was performed in nc/scCO$_2$ at pressures ranging from 7.8 to 14 MPa under normal and μg conditions to afford **1E** in ee which was highly pressure-dependent (Fig. 3). Thus, the product's ee rapidly increased with increasing pressure up to 11 MPa and then leveled off in both cases. However, the pressure-dependence profile was not identical in the two cases and appreciably higher ee values were obtained under μg particularly in the near critical region (9-10 MPa), demonstrating that the stereochemical outcomes can be manipulated by performing chiral photoreactions in nc/scCO$_2$ under μg. Mechanistic details will be discussed in the presentation.

References

1) Y. Inoue, E. Matsushima, T. Wada: J. Am. Chem. Soc., 120, (1998) 10687.
2) R. Saito, M. Kaneda, T. Wada, A. Katoh, Y. Inoue: Chem. Lett., (2002) 860.

リング状液膜内マランゴニ対流現象に及ぼすメニスカス形状の影響に関する数値解析

山本卓也，○高木洋平，伴貴彦，岡野泰則（大阪大学），水口尚（琉球大学）

Numerical Simulation of the Effect of the Meniscus Shape on Marangoni Convection in a Ring-Shaped Liquid Film

Takuya YAMAMOTO, Youhei TAKAGI, Takahiko BAN, Yasunori OKANO (Osaka Univ.),
Hisashi MINAKUCHI (Univ. of the Ryukyu)

1. Introduction

Thermocapillary and Marangoni flows are driven by surface tension gradients along free surfaces and the flows become remarkable under micro-gravity fields.

Onboard ISS, D. Pettit conducted an experiment in a thin water film sustained in a circular stainless wire ring[1]. When a section of the ring was heated, a thermocapillary flow developed in the liquid film towards the heated region. This was contrary to what predicted theoretically.

To shed light on the mechanism determining the direction of the thermocapillary flow in a thin circular film, we conducted a three-dimensional numerical simulation. In the simulation, we focused on the effects of meniscus shape and wire curvature.

2. Numerical analysis

The governing equations of liquid phase are the momentum, continuity, and energy balance equations. Along the free surface, thermocapillary force is in effect and the velocity gradient in the normal direction to the free surface is proportional to temperature gradient. The free surface is assumed to be adiabatic. On the wire wall, no-slip condition was imposed, and temperature boundary condition is analytically approximated by one-dimensional unsteady heat conduction. The detail of the other numerical procedures is found in T. Yamamoto *et al.*[2].

Three computational domains are prepared to investigate the effects of meniscus and wire curvature. **Fig. 1** shows the schematics of computational domains. The film diameter is 10 mm; that is small compared with the space experiment because of save of numerical cost.
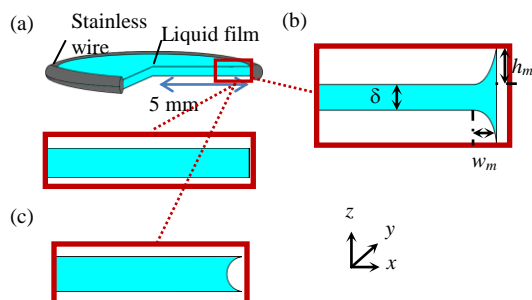

Fig. 1 Schematic diagram of film shape: (a) flat, (b) meniscus, and (c) wire curvature.

3. Results and Discussions

In the case of **Fig. 1** (a), the flow pattern was roll flow near heated wire. Symmetric vortex pair emerged near wire. In the case of **Fig. 1** (b), meniscus shape changed flow pattern. For $h_m/w_m \gg 1$, the flow toward heat source developed. For $h_m/w_m \ll 1$, the flow toward center of frame developed. When $h_m/w_m \approx 1$, both flows were observed. In the case of **Fig. 1** (c), the flow toward heat source was developed. **Fig. 2** shows the experimental and numerical results of particle tracers when numerical condition of film diameter corresponds to the experiment. These numerical results show a good agreement with the experimental result.

When the flow pattern corresponded to space experiment, symmetric vortex pair developed near heated wire, and the vortex was stretched in circumferential direction. The flow depended on temperature gradient along the free surfaces. A steep temperature gradient in radial direction caused the occurrence of symmetric vortex pair. Then, the vortex pair was stretched by circumferential temperature gradient.
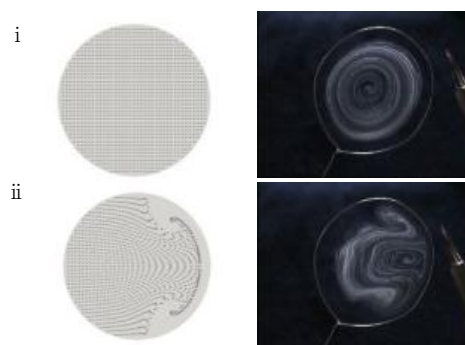
Fig.2 Snapshots of particle tracers for numerical (left) and experimental (right) results: (ⅰ) initial, and (ⅱ) after heating.

4. Conclusion

Thermocapillary flow in a thin film was numerically investigated. The meniscus shape and wire curvature changed the flow direction, and the flow pattern depended on the temperature gradient along the free surfaces.

References

1) D. Pettit: Saturday Morning Science Videos (2003).
2) T. Yamamoto, Y. Takagi, T. Ban, Y. Okano, H. Minakuchi, and S. Dost; Proc. 23th Int. Symp. Transport Phenomena, 2012.

微小重力環境において液柱形状がマランゴニ対流のモード構造に与える影響

○矢野大志，西野耕一（横浜国立大学），河村洋（諏訪東京理科大学），上野一郎（東京理科大学），
松本聡，大西充（宇宙航空研究開発機構）

Effect of Liquid Bridge Shape on the Mode Structure of Marangoni Convection under Microgravity

Taishi YANO, Koichi NISHINO (Yokohama National Univ.), Hiroshi KAWAMURA (Tokyo Univ. of Science, Suwa), Ichiro UENO (Tokyo Univ. of Science), Satoshi MATSUMOTO, Mitsuru OHNISHI (JAXA)

1. Introduction

A number of microgravity (μg) experiments on the Marangoni convection have been conducted so far. Marangoni convection is the flow that driven by the surface tension gradient along a liquid-gas interface and this flow becomes important and dominant under the μg environment because of the absence of density driven flows. A series of MEIS (Marangoni Experiment in Space) have been started as the first science experiment on the "Kibo" in 2008 [1]. The aim of MEIS is to understand the instability mechanisms of Marangoni convection and several parameters are considered. In this study, effects of the liquid bridge shape on the mode structure and instability of Marangoni convection are discussed.
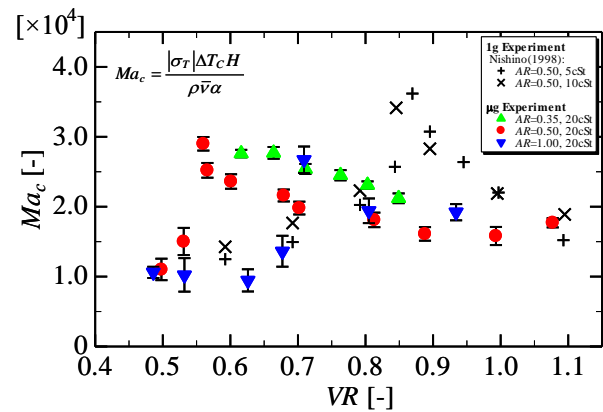
2. Experiment

In the present experiment, Marangoni convection takes place inside the liquid bridge that is suspended between coaxial heated and cooled disks. A wide range of aspect ratio, AR (=H/D), can be realized by traversing the cooled disk in axial direction, where H and D are the length of the liquid bridge and the diameter of the disk, respectively. The overview of the liquid bridge is viewed with a colored CCD camera, and the liquid bridge shape is controlled by adjusting the fluid volume by the bellows placed behind the cooled disk. Volume ratio, VR (=V/V_0), is used to collect the effect of liquid bridge shape, where V and V_0 are the volume of liquid bridge itself and that of the gap between disks ($V_0 = \pi D^2 H/4$), respectively. It is known that the liquid bridge shape is uniquely determined by AR, VR and Bond number, Bo [2].

3. Results and Discussion

In the present experiment, three different ARs (i.e. 0.35, 0.5, 1.0) are chosen to study the effect of liquid bridge shape. **Figure 1** shows the liquid bridge shapes corresponding to VR=0.50, 0.81 and 1.08 for AR=0.5. The liquid bridge shape changes from concave to convex with increasing VR. The measured critical Marangoni number, Ma_c, is plotted as a function of VR in **Fig. 2**. Also included in **Fig. 2** are the literature data [3] that is obtained in terrestrial (1g) experiments. It is widely known that VR

| VR=0.50 | VR=0.81 | VR=1.08 |
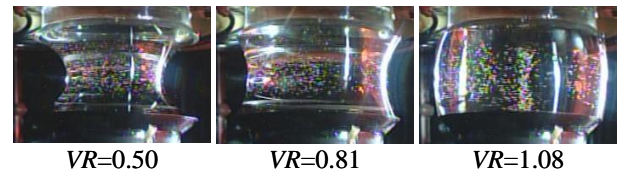
Fig. 1   Shape of liquid bridge for different VR

Fig. 2   Plot of Ma_c as a function of VR

strongly affects the Marangoni instability. As shown in **Fig. 2**, Ma_c changes with changing the VR. In the case for AR=0.5, the results from μg experiment show local peak at VR=0.55, while such a local peak exist at VR=0.85 in the 1g experiment. Moreover, observed mode structures of Marangoni convection are also different between the μg and 1g experiment. Under μg condition, azimuthal mode number, m, equal to 1 around VR=0.50~1.08. While under 1g condition, m equal to 1 around VR=0.90~1.10, but it changes at local peak and m equal to 2 is observed around VR=0.60~0.87. This different should be caused by the effect of buoyancy.

References

1)   H. Kawamura, K. Nishino, S. Matsumoto and I. Ueno: J. Heat Transfer, **134** (2012) 031005-1.

2)   L. A. Slobozhanin and J. M. Perales: Phys. Fluid A, **5** (1993) 1305.

3)   K. Nishino, T. Kitagawa and S. Yoda: Marangoni Convection Modeling Res., (1999) 37.

可視化法を用いた微小重力中の超流動ヘリウムと常流動ヘリウムのプール沸騰熱伝達の研究

○高田　卓（筑波大学），木村　誠宏（高エネルギー加速器研究機構），間宮　幹人（産総研），

岡村　崇弘（高エネルギー加速器研究機構），野澤　正和（秋田高専），村上　正秀（筑波大学）

Study of Pool Boiling Heat Transfer in Superfluid Helium and Normal Liquid Helium under Microgravity by using Visualization Method

Suguru TAKADA (Univ.of Tsukuba), Nobuhiro KIMURA (KEK), Mikito MAMIYA (AIST), Takahiro OKAMURA (KEK), Masakazu NOZAWA(Akita National Tech.), Masahide MURAKAMI (Univ. of Tsukuba)

1. Introduction

Superfluid helium (He II) is used as a coolant for astronomy satellite such as X-ray telescope[1]. Thus the investigation of He II heat transfer has been required. It is well known that the critical heat flux of He II is strongly dependent on small subcooling due to hydrodynamic pressure head. Under µg environment, the subcooling of He II would be absolutely zero so that the present experiment would be very important.

Therefore the present experiment was carried out by using drop-tower in order to understand He II film boiling under microgravity condition. Small cryostat equipped with optical windows and visualization system was embedded in the capsule of the drop tower at Hokkaido center of AIST. And in the case of normal liquid helium (He I), the film boiling experiment was also carried out for comparison.

2. Experimental Apparatus and Drop Tower in Hokkaido Center, AIST

We designed the small cryostat equipped with optical windows for the experiment using by the drop tower[2]. The test vessel is about 5 litters. A thin manganin wire heater of φ50 µm was set horizontally. Electric resistance of manganin has positive relation with temperature at low temperature. Thus a thin wire heater was also used as a thermometer. The heat current has applied with the constant power supply that has a feed-back control was used for fixed heat flux condition. The high speed camera was used in this present study. The frame rate had been 231 frames/sec. The flat LED light illuminates from the side of a window glass and the high speed camera with telecentric lens was set opposite side.
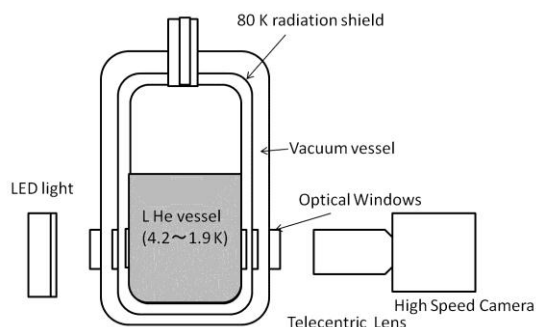

Fig.1 Rough sketch of optical setup.

as shown in **Fig.1**. The time duration of microgravity environment below 1 mili-g is about 1.3 sec.

3. Visualization Results

In He II film boiling, the very thin vapor film was formed and vapor bubble was never departed on 1G. The thickness of vapor film is about 0.2 mm. On the other hand, vapor film was getting much larger more than 20 mm under µg condition as shown in **Fig. 2** (a) and (b). The nucleate boiling state was never observed under µg as same as on 1G.

The typical visualization results of He I boiling were shown in **Fig. 3**(a) and (b). It is found that nucleate boiling and film boiling can be recognized clearly. In nucleate boiling state, small vapor bubbles departs from thin heater wire. On the other hand, in film boiling state, vapor bubbles formed large bubbles of about 6 mm diameter and small oscillating bubble of 1mm diameter periodically. And the vapor bubbles never depart from wire heater.
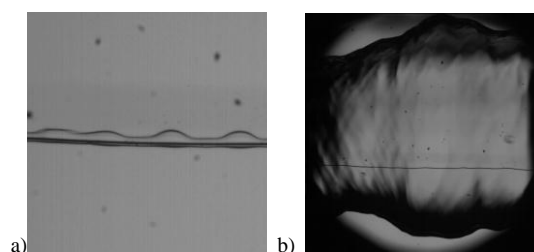

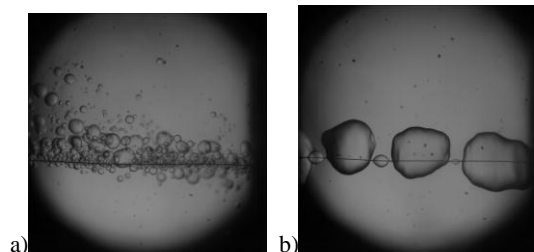**Fig2** visualization results of He II film boiling at 1.9 K, q = 22.3 kW/m^2 (a) 1G (Zoom up x4) (b) under µg.

Fig.3 typical visualization results of He I at 4.2 K under µg (a) nucleate boiling q=9.70 kW/m^2 (b) film boiling q=22.3 kW/m^2.

References

1) Fujimoto R., Mitsuda K., *et. al.*, Cryogenics **50** (2010) 488.

2) N. Kimura, S. Takada, S. Gotoh, H. Kawamata, M. Iida, M. Murakami, H. Nagai and M. Mamiya, Cryogenics**51** (2011)74.

温度差マランゴニ効果による懸垂液滴内粒子挙動と Hydrothermal wave 不安定性

○渡邉拓実，上野一郎 (東京理科大学)

Particle behavior and hydrothermal wave instability
in hanging droplet due to thermocapillary effect

Takumi WATANABE, Ichiro UENO (Tokyo Univ. of Science)

1. Introduction

We has been focusing on thermocapillary-driven convection in a hanging droplet with experimental approaches[1]. We realize a transition of the flow field from a two-dimensional steady flow to three-dimensional time-dependent 'oscillatory' ones. The oscillatory flow is accompanied with a thermal wave traveling over the free surface at a constant frequency. Such a thermal wave induced by the thermocapillary effect is known as the hydrothermal wave instability[2] (HW, hereafter). In the present research, we evaluate the transition point of the flow inside the droplet, and the fundamental frequency of the oscillatory flow after the transition. We make a comparison of the present data with the ones by on-orbit experiments in the Japanese Experimental Module 'Kibo' aboard the International Space Station[3].
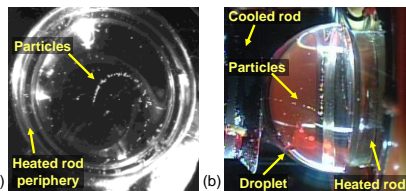

Fig. 1 Example of view obtained by one of the top view cameras (a) and side view camera (b) in on-orbit experiments (MEIS-3)

2. Experimental condition

The droplet is formed on the top rod facing downward, and the bottom rod is placed beneath the droplet. We use two kinds of top rods, whose radius is of 1.0 and 1.5 mm. The test fluids are 2 and 5-cSt silicone oil with Prandtl number Pr of 28.1 and 68.4 at 25 °C, respectively. The physical properties of the fluid are listed in Table 1. We observe the flow fields with two high speed CMOS cameras, and simultaneously measure the surface temperature with an infrared camera (IR camera) whose frame rates are 60 fps.

3. Results and Discussion

The intensity of the flow induced by the thermocapillary effect is described by using a non-dimensional Marangoni number Ma ($=(\sigma_T \Delta T(V/R^2))/\rho\nu\kappa$), where σ_T is temperature coefficient of surface tension, ΔT is temperature difference of both rods, V is volume, R is radius of the top rod, ρ is density, ν is kinematic viscosity, κ is thermal diffusivity. We detect them in variations of the R of the rods and of the Prandtl number Pr of the test fluid. The critical marangoni number Ma_c increases monotonically when the aspect ratio Γ (=H/R) decreases at each experimental condition; it is found that the Ma_c is well described with Γ. Results of MEIS-3 are in good agreement with terrestrial experiments. The non-dimensional frequency F ($=(H^2/\kappa)*f$) is plotted against Ma. It is clearly seen that the F exhibits a condensed manner against the Ma almost independently of R and Pr. The results obtained in MEIS-2 and MEIS-3 are in good agreement with the terrestrial experiments in spite of rather large differences of R and Pr.

References
1) T. Takakusagi, I. Ueno, and C. Hong, Bulletin European Low Gravity Research Association **27** (2010) 32.
2) M. K. Smith and S. H. Davis, J. Fluid Mech. **132** (1983) 11.
3) H. Kawamura, K. Nishino, S. Matsumoto, and I. Ueno, J. Heat Transfer **134** (2012), 295.
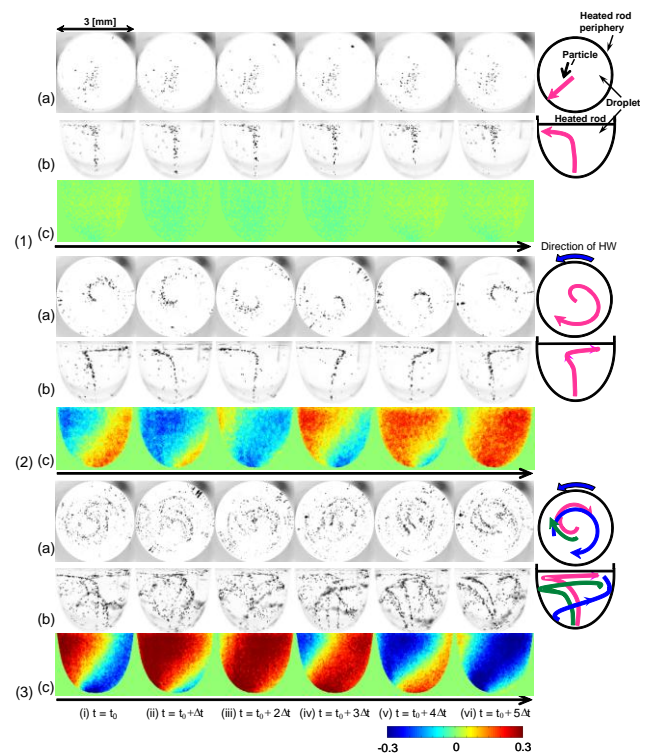
Fig. 2 Time series of snapshots of each flow regimes; (1) Steady flow, (2) Traveling flow, and (3) Dynamic PAS flow at time interval Δt [s] of (1) 0.372, (2) 0.178 and (3) 0.117, respectively. Spatio-temporal correlation between particle line observed (a) from above, (b) from side, and (c) the surface temperature deviation observed from another side, respectively. The temperature difference in snapshots of temperature deviation is ± 0.3 [K]. The HWs of (2) the Traveling wave and (3) the Dynamic PAS flow propagate from the left to the right in the frame (i.e., counterclockwise) in these cases. Schematic views are drawn aside the last image of particle lines. Outer circle in the top view corresponds to the periphery of the top rod whose radius is 1.5 mm.

強い重力場を用いた反ポーリング則構造を持つ TiO₂ の合成

○ 真下　茂、Rabaya BAGUM、緒方雄大（熊大）、奥部真樹（東工大）、杉山和正（東北大）、
磯部　博志（熊大）、吉朝　朗（熊大）

Synthesis of Anti-Pauling Structure Rutile (TiO₂) Produced under Strong Gravitational Field

Tsutomu MASHIMO, Rabaya BAGUM, Yudwai OGATA(Kumamoto University), Maki OKUBE(Tokyo Instt. Tech.),
K. SUGIYAMA(Tohoku University), Hiroshi ISOBE, Akira YOSHIASA(Kumamoto University)

1. Introduction

Rutile type $TiO_2(D_{4h}^{14})$ essentially consists of edge-sharing distorted TiO_6 octahedral groups (Ti-Oa -1.947 Å, and Ti-Ob:1.9808 Å) and Ti ions form a tetragonal lattice which is compressed along with c-axis. We have investigated the effect of application of a strong gravitational field during heat treatment on the crystal structure and properties of single-crystal rutile (TiO2) using the high-temperature ultracentrifuge[1]. Under a strong gravitational field (~10^6 G level), heavy atoms are displaced in the gravitational direction, and light atoms in the opposite direction by the different body forces relative to respective atomic weight in compound crystal. Under such conditions, a unique atomic strain further the nonequilibrium crystalline state would appear, and a metastable form might be quenched to ambient condition.

2. Experimental procedure

Single crystal plate specimens, 5 mm diameter and 1 mm thick were set on a sapphire plate in a stainless steel SUS304 capsule. The gravitational field was applied along the c-axis of the crystal with the maximum distance from the rotor axis being about 35.5 mm. The gravity at the sample for a rotation velocity of 100,000 rpm was $(0.39-0.40) \times 10^6$ G. The rotor was radiatively-heated to 400°C by a hot carbon, hollow cylinder which in turn was heated by a high frequency heating system. The duration was 24 hours. Single-crystal X-ray diffraction measurements for crystals were carried out with a four-circle diffractometer at the BL-10A beam line of the Photon Factory. Structure refinements were performed by minimizing the function $\sum w (|F_o| - |F_c|)^2$ using a full matrix least-squares program, RADY (23).

3. Results and discussion

Figure 1-a shows comparisons of the c/a ratios obtained by gravity with those from pressure [2] and temperature [3] variations. The axial ratio c/a increases with increasing pressure i.e., the a-axis is more compressible than the c-axis. For the centrifuged sample, the lattice constant c decreased (0.3%) and a increased (0.05%); thus the c/a ratio decreased, and the structure became more anisotropic. The changes in lattice constant may also be related to the fact that gravity is body force and was applied along the c axis.

Figure 1-b shows the ratio of the distances Ti–Oa and Ti–Ob of the rutile phase, and compares the effect of gravity treatment with those of pressure [4] and temperature [3]. The Ti–Oa and Ti–Ob distances in the present sample increased by 0.7 % and decreased by 0.9 %, respectively. The ratio of these two interatomic distances increased, and approached 1 (0.997). To obtain the same state using pressure, we would need to apply over 140 GPa. In the

present sample, Os and Ou are 2.613Å (3.2% enlarge than for standard rutile) and 2.7728Å (0.16% less than standard rutile), respectively. As a result, Os/Oa approached 1 (0.9224), implying a more isotropic state. It is notable that the $Ti-O_6$ octahedral structure approaches the isotropic state, which is against Pauling's rules.
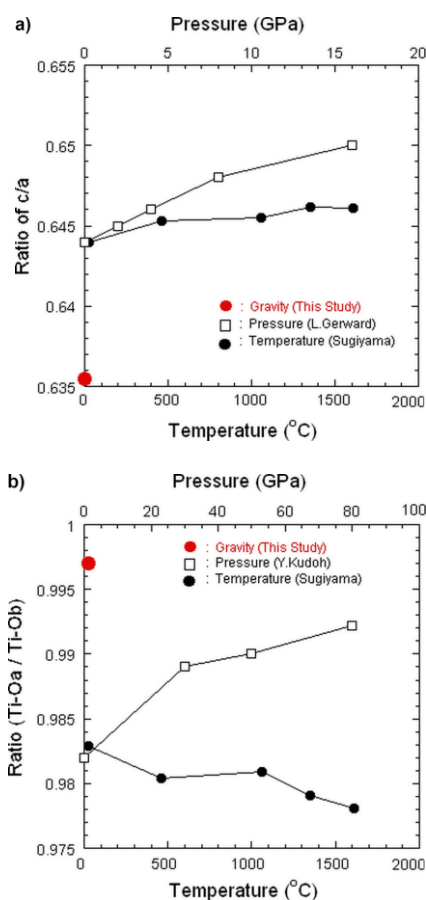
Fig. 1 The c/a (a) and Ti–Oa / Ti–Ob (b) ratios for rutile of the gravity sample as compared with pressure [3] and temperature dependences [4].

We could stress a bit more that this method is general and could be applied to many common materials; it produces very different results than static high pressure and at least based on this work it overcomes many of the difficulties associated with producing new materials.

References

1) T. Mashimo *et al.*, *Rev. Sci. Instr.* **74**, 160 (2003).
2) L. Gerward, J. Staunolsen, *J. Appl. Cryst.,* **30**, 259 (1997).
3) K. Sugiyama, Y. Takeuchi, *Zeitchrift Fur Kristallographie,* **194**, 305, (1991)**.**
4) Y. Kudoh, H. Takeda, *Physica B.* **139-140,** 333, (1986).

強い重力場下における拡散対の界面拡散

○ 緒方裕大、近藤慶祐、坂田祐樹、井口裕介、真下茂（熊本大学　真下研究室）

Diffusion Phenomenon at Interface of Metal Couples under a Strong Gravitational Field

Yudai OGATA, Keisuke KONDO , Yuki SAKATA, Yusuke IGUCHI, Tsutomu MASHIMO (Kumamoto Univ.)

1. Introduction

To know advantage of microgravity, we should know about the gravity effect. Strong gravity is suitable for the study of the gravity effect and would reveal the gravity effect in more visible form.

Electronic device such as semiconductor or metal or etc. is indispensable for life and development of human civilization. The interface is important for functionality of the electronic device. So, we need control interface at atomic-scale for development of new electronic device.

The experiment of diffusion using the Copper-Brass diffusion couple was performed by Dr. Kirkendall in 1947[1]. He found the vacancy mechanism; it is not only substitution and interstitial ones and it is called Kirkendall effect. So, this Copper-Brass diffusion couple is very famous example.

In this study, we performed the strong-Gravity experiment on Cu-Brass couple to study the interface diffusion phenomena.

## 2. Experimental procedure

We prepared We prepared metal couples of Cu/Brass (Cu:Zn=70:30 at. %) using the electroplating method. Then we have gotten copper-plated Brass at the cathode about 2mm in thickness. Copper-plated Brass was cut into specimens of approximately 5 mm in diameter and appearing interface clearly. We prepared two type samples, one is that Copper was upside and Brass was downside, and another is that Brass was upside and Copper was downside. In this study, we used plate type capsule. As a result, interface of specimens were applied the centrifugal force vertically. The rotor can be heated by a hot carbon, hollow cylinder which in turn is heated by a high frequency heating system. Experimental conditions are summarized in **Table 1**. We performed also the annealing experiment at 1G, the same temperature, and for the same time duration to compare with usual thermal diffusion. The composition analysis was performed using electron probe micro analysis with a JXA-800R (Japan Electron Optics Laboratories Co., Ltd).

Table 1 Experimental condition

Rotation speed (rev×min⁻¹)	Maximum acceleration (×10⁶G)	Temperature (℃)	Time (h)
100 000	0.4	400	60

3. Results

Figure 1 shows EPMA color mapping of Copper-Brass after ultracentrifugal experiment. The black area in figure indicates nothing Zinc, and containing many Zinc when color move toward warm color. Experimental gravity direction was upside: Copper and downside: Brass. We confirmed that interface between Zinc contained in Brass and Copper blurred the same phenomenon as annealing experimental result. We compared ultracentrifuged Cu-Brass chart with annealed one chart, then, we found that the composition gradient at the interface of ultracentrifuged Cu-Brass was gentler than the annealed one. On the other hand, when gravity direction was upside: Copper and downside: Brass. We observed that the composition gradient at the interface of ultracentrifuged Cu-Brass steeper than the annealed one. So, we considered thermal diffusion and sedimentation under strong gravitational field. In case of upside: Copper gravity direction, first, Copper and Zinc move to another metal due to the thermal diffusion. Then, because of a gravitational field, Copper atoms move to the gravity direction. Zinc atoms move to the opposite direction. So, the movement of Copper under the gravitational field enhanced the thermal diffusion. Just the same, in upside: Brass case, the movement of these atoms under the gravitational field blocked the thermal diffusion. As a result, in a strong gravity field, gravity effect can control the thermal diffusion.
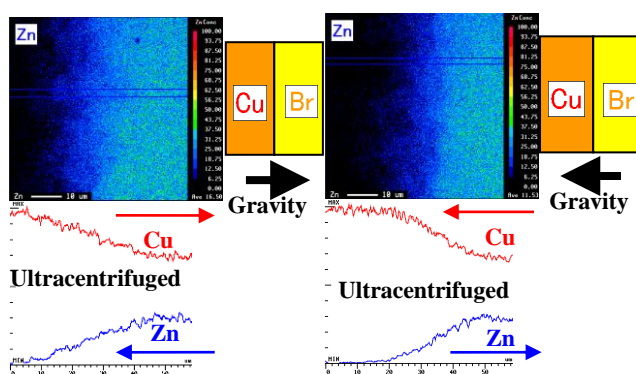
Fig.1 The concentration distribution of the ultracentrifuged Cu-Brass Left(Upside: Cu and Downside: Brass) Right(Upside: Brass and Downside: Cu)

References

1) A. D. Smigelskas and E. O. Kirkendall: Zinc Diffusion in Alpha Brass. Trans. AIME, 171 (1947), 130-142.

強い重力場を使った機能熱電傾斜材料の作製

○Januszko KAMILA (AGH University, 熊本大学), Wojciechowski KRZYSZTOF,
Zybala RAFAL (AGH University, Poland), 緒方裕大, 真下茂 (熊本大学)

Preparation of Functionally Graded Thermoelectric Materials under Strong Gravitational Field

Kamila JANUSZKO (AGH University, Poland; Kumamoto University, Japan), Krzysztof WOJCIECHOWSKI,
Rafal ZYBALA (AGH University, Poland), Yudai OGATA, Tsutomu MASHIMO (Kumamoto University, Japan)

1. Introduction

Thermoelectric materials can be used for the conversion of heat energy into electricity. They found application e.g. in independent power supplies, so called thermoelectric generators TEG, that do not need maintenance for many years (e.g. in space probes Voyager [1, 2]. However, the efficiency of the commercially available materials is that of only around 5%, what limits their common applications in daily use.

Thermoelectric materials efficiency and their properties depend on carriers' concentration and temperature, however increasing temperature gradient is limited by physical properties of the material. Therefore gradation of the carriers' concentration inside the material seems to be the best solution. As a result of gradation, efficiency of the material should increase significantly comparing to uniform material.

A strong gravitational field realized the sedimentation of atoms in solid, i.e. an atomic-scale graded structure[1, 2]. Kumamoto University ultracentrifuge apparatus can generate an acceleration over one million G ($1G=9.8m/s^2$) at high temperatures. Previous research of grading different materials using these apparatus gives high expectations of applying this method for the research.

This research concentrates on preparation of functionally graded thermoelectric materials to enhance their properties and efficiency, using gravitational field as a grading factor.

To perform effective gradation the material with heavy and light atoms is required. Then, according to gravity force movement of light atoms in the direction of gravity force and heavy atoms against this direction can be observed. For this reason the thermoelectric materials of $AgSbSe_2$ and $BiSbTe_3$ were used. Both of these are very good thermoelectric materials. Especially $AgSbSe_2$ was interesting for this research, according to its unusual properties[3, 4].

2. Experimental and results

Experiment was performed using ultracentrifuge apparatus with conditions of 120 000 rot/min in 400°C for both samples.

Change in chemical structure in materials was confirmed using EPMA analysis.

For estimating thermoelectric material efficiency, usually ZT value (figure of merit) should be calculated:

$$ZT = \frac{\alpha^2 \cdot \sigma}{\lambda} \cdot T_{aver}$$

where α-Seebeck coefficient, σ-electric conductivity, λ-thermal conductivity, T-temperature.

Optimization of given thermoelectric properties allows to get highest possible ZT for the material. For this study thermoelectric properties analysis Seebeck coefficient as a representative thermoelectric property was measured using STM (Scanning Thermoelectric Microprobe) (AGH University, Poland).

Experimental results show small gradation in chemical structure for both materials that were previously uniform. As Seebeck coefficient differences can be seen even due to small change in carriers' concentration, more significant effect is visible. Gradation effect on the samples can be observed on the following figure (**Fig.1.**)

a)   b)
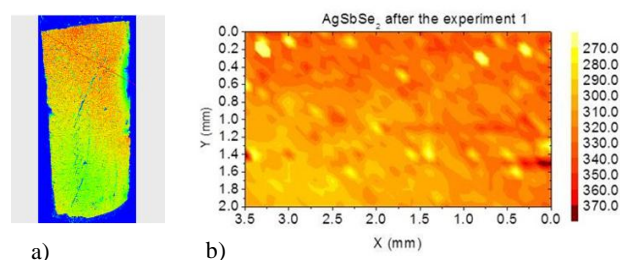
Fig.1. $AgSbSe_2$ sample after the high gravity experiment at 120 000 r/min, 400°C: a) EPMA analysis, b) colour map of Seebeck coefficient distribution

4. Conclusions

The change in chemical structure and thermoelectric properties were observed. Other thermoelectric materials should also be investigated. Longer time of performing the experiment can be considered for more significant effect.

References

1) T. Mashimo, Phys. Rev. A **38**, 8, (1988) 4149

2) T. Mashimo, Acta Astronaut. **48**, (2001). 145

3) K.T. Wojciechowski and M. Schmidt, Phys. Rev. B **79**, (2009) 184202

4) K. Wojciechowski, M. Schmidt, J. Toboła, M. Koza, A. Olech, R. Zybala, J. of Electr. Mat., Vol. **39,** No. 9, 2010, 2053-2058

過冷却融液からの Cr-Si 系熱電材料の合成

○永井秀明（産総研）、濱田　剛、奥谷　猛（横国大大学院）

Synthesis of Cr-Si Thermoelectric Material by using Undercooled Melt

○Hideaki NAGAI (AIST), Tsuyoshi HAMADA, Takeshi OKUTANI (Yokohama Nat. Univ.)

1. Introduction

$CrSi_2$ is known as a candidate for thermoelectric applications, and has been reported to have large anisotropy of thermoelectric properties against c-axis[1]. To synthesize thermoelectric Cr-Si alloy with higher performance, it is important to control both crystalline alignment and metallurgical structure. Our previous works has revealed that the structure control of Si-Ge alloy and ZrNiSn alloy solidified in microgravity are useful to improve their thermoelectric performance[2,3]. Recently, we have synthesized Si-Ge alloy with metallurgical structure and crystalline alignment solidified from undercooled melt using electromagnetic levitation (EML) method. In this study, we investigated the synthesis of Cr-Si alloys by using EML method.

2. Experimental

Cr-Si alloys with different Cr/Si ratio were prepared by arc-melting from the constitute elements. 5 at% of Cr component was substituted by V as a dopant.

Our EML equipment has He gas cooling system, and the melt sample can be cooled during levitation. The sample was levitated in Ar gas flow at first, and kept above melting point (m.p.) for 2 min. The sample was cooled down by introducing He gas. When the melt temperature was reached around 1680 K, lower than m.p. of $CrSi_2$ (1763 K), the sample was solidified by contact of Si chill block. The structure of the solidified sample was analyzed by XRD, OM and SEM. The thermoelectric properties was evaluated by electrical conductivity, Seebeck coefficient and thermal conductivity.

3. Result and discussion

All samples with different Cr/Si ratio could be levitated by EML method. Several samples could be cooled down around 1680 K without solidification by introducing He gas, but the sample with 44at% Cr component could not be cooled down below m.p, even though introducing He gas of more than 200 ml/min.

Figure 1 shows the cross sections of $CrSi_2$ solidified from the melt by different solidification method. The sample solidified from undercooled melt had fine metallurgical structure without crystalline alignment. This result revealed that solidification rate from the melt with undercooled degree of 70 K was so fast that the sample was randomly solidified. On the other hands, the arc-melted sample had large grains and many cracks in the

sample. From the XRD pattern, the arc-melted sample was considered to be a mixture of large grains with crystalline alignment. The samples with different Cr/Si ratio solidified from undercooled melt also had fine metallurgical structure without crystalline alignment.
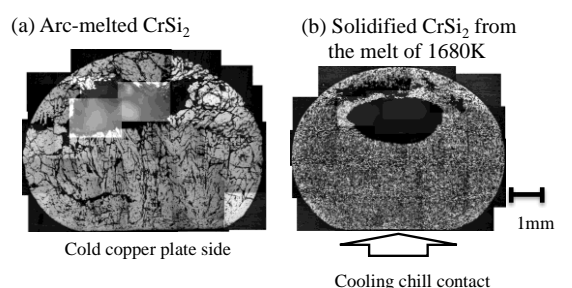

(a) Arc-melted $CrSi_2$ 　(b) Solidified $CrSi_2$ from the melt of 1680K

Cold copper plate side　　Cooling chill contact　1mm

Fig.1 Cross section of $CrSi_2$ sample solidified from the melt.

Table 1 shows the thermoelectric properties of the sample with different Cr/Si ratio at 900 K. All arc-melted samples had lower electrical conductivities because of cracks in the sample. Cr-rich sample had higher electrical conductivity because this sample was a mixture of $CrSi_2$ and CrSi phase and CrSi phase is a metallic phase. On the other hands, Cr-poor sample had lower electrical conductivity because this sample was a mixture of $CrSi_2$ and Si phase and this Si phase was a semiconductor phase without doping. The Seebeck coefficients of the $CrSi_2$ samples were similar to those of Cr-poor sample because of the same V-doping concentration in $CrSi_2$ phase. The lower Seebeck coefficient of Cr-rich sample was caused by increasing V-doping concentration in $CrSi_2$ phase, because V was rarely dissolved in CrSi phase.

Table 1 Thermoelectrical properties of Cr-Si alloys at 900 K

	Cr compoment (included V)	36	33.3	29
Solidified sample from undercooled melt	Electrical conductivity (S/m)	2.44E+05	4.45E+04	2.47E+04
	Seebeck coefficient (mV/K)	62.5	109	102
	Thermal conductivity (W/mK)	non-measurement	2.41	non-measurement
	ZT	-	0.20	-
Arc-melted sample	Electrical conductivity (S/m)	2.72E+04	2.04E+04	1.60E+04
	Seebeck coefficient (mV/K)	56.8	1.11E+02	100

References

1) I. Nishida: J. Mater. Sci., **7** (1972) 1119.
2) T. Okutani, Y. Kabeya, H. Nagai: Proc. 7th Interdisciplinary Transport Phenomena Conference, Dresden/Germany, Sep. 2011, 13-3.
3) H. Nagai, R. Muroi, T. Okutani: J. Phys, **327** (2011) 012008-1.

チタニアナノスケルトンの微小重力下における調製とその物性

○遠藤健司、酒井秀樹、阿部正彦、（東京理科大学）畠山望、宮本明、（東北大学）
酒井俊郎、（信州大学）羽生直人、（資生堂リサーチセンター）坂本一民、（千葉科学大学）福井寛、
（福井技術士事務所）勝田真登、越川尚清（宇宙航空研究開発機構）

Preparation of Titania Nanoskeleton in Microgravity and Its Properties.

○Takeshi ENDO, Hideki SAKAI, Masahiko ABE, Nozomu HATAKEYAMA, Akira MIYAMOTO, Toshio SAKAI, Naoto HANYU, Kazutami SAKAMOTO, Hiroshi FUKUI, Masato KATSUTA, Naokiyo KOSHIKAWA

1.Introduction

Synthetic inorganic mesoporous materials like MCMs have various potential applications due to their regularly arranged mesopores. Among such mesoporous materials mesoprous titania is expected as a candidate for novel photocatalyst, chemically stable molecular sieve and so on. Although generally crystalline titania is obtained through heating of amorphous particles, we succeeded in synthesis of crystalline mesoporous titania near room temperature by using a quarternary ammonium type cationic surfactant as a structure directing agent and named the obtained material as titania nanoskeleton. We attempted synthesis of titania nanoskeleton in microgravimetric environment.

2. Experimental

Titanium oxysulfate and trimethyl benzene (TMB) aqueous suspension / cetyltrimethylannonium bromide (CTAB) aqueous solutions are packed separately in three fold polyethylene bag before launch. (**Fig. 1**) Sample bags were stowed in refrigerator before experiment in ISS. Sawed precursors were mixed together and followed by 3 days reaction at 40℃. Obtained particles are analyzed after filtration and drying on ground. Mesoporous structure was investigated by transmission electron microscopy and small angle X-ray scattering. Pore diameter was investigated by nitrogen gas adsorption desorption measurement at 77 K. Photo catalytic activity was examined for isopropanol gas decomposition.
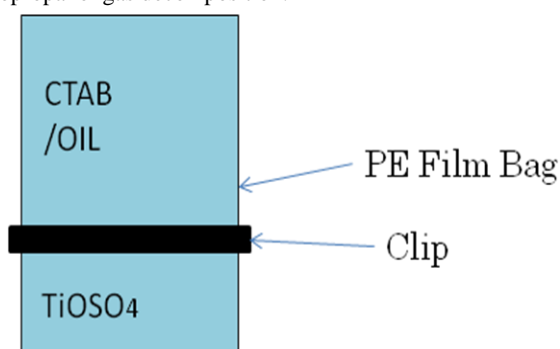

Fig. 1 Appearance of sample mixing bag. Clip separates the precursor solutions until the experiment starts.

3. Results and discussion

All samples were successfully retrieved. The appearance of the samples was almost the same with that of terrestrial controls. SAXS patterns show that nanoskeletons prepared in ISS also shows hexagonal mesoporous structure. The interpore distance increased as compared with terrestrial controls as shown in **Fig. 2**. In the cases of the samples prepared without TMB, regularity of the porous structure improved significantly. Anatase crystalline sizes of the framework were almost same for both cases. Diameter of the aggregates reduced in 2-30 % by SEM observation. These results show that microgravity environment has significant effect on interpore distance of the nanosleletons prepared with oil phase (TMB), while uniformity of the pore is improved for the samples prepared. And photocatalytic activity improved for the samples that has more ordered structure.
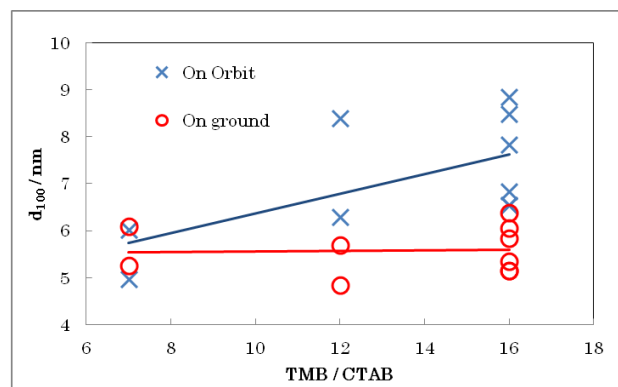

Fig. 2 Pore to pore distance (d_{100}) of the obtained nanoskeletons with various TMB/CTAB ratio. ○ represents the d_{100} values of terrestrial control samples and × represents those of the samples obtained in microgravity.

References

(1) H. Shibata et al, *J.Am.Chem.Soc.***127**, 16396 (2005)